A modeling investigation of the calcium dynamics underlying human EEG signals

by

Sarah Pugliese

Thesis Advisor: Dr. Stephanie Jones, Department of Neuroscience
Second Reader: Dr. Matthew Harrison, Division of Applied Mathematics

Submitted to the Division of Applied Mathematics in partial fulfillment of the requirements for Honors

April 2020

Abstract

Electroencephalography (EEG) signals are created by electrical currents from pyramidal neurons in the outer layer of the brain. These signals are easy to obtain and can provide useful biomarkers for clinicians, but little is known about how the underlying network activity in the brain generates the waveform features of the EEG. Our lab has developed a computational model to study this relationship. Dendritic calcium spikes are a well-characterized phenomenon in layer 5 pyramidal neurons, and are potentially significant contributors to EEG signals, but our model did not accurately account for this type of dendritic activity. In this thesis, I describe my process of updating the model layer 5 pyramidal neurons to better fit experimental recordings, then examine the effects of calcium events on the simulated source-localized EEG signal. I was able to replicate findings that dendritic calcium spikes have a distinct signature in surface recordings, and found that generally the sustained electrical activity in the distal dendrites during a dendritic calcium spike pushes a significant amount of current down the apical dendrite. Particularly in the case of strong excitatory inputs which evoke many near-synchronous calcium spikes in the local network, the resulting downward current cannot be accounted for without calcium-mediated activity. This new understanding of electrical activity in the dendrites improves the accuracy of the model and will help future efforts to use this model to interpret real EEG data.

Contents

Chapter 1

Biophysical Neural Modeling

1.1 Electrical activity in the brain

The human brain is made up of billions of neurons, a class of cells that are able to receive and send electrical impulses through branch-like projections called dendrites and axons. These electrical signals are generated by ion channels in the cell membranes of neurons which, when open, allow ions of different types to flow into or out of the cell. Many of these channels are voltage-gated, meaning that they open or shut when the membrane's voltage reaches a certain level. In their resting state, most neurons have a membrane voltage around -65 mV, and they have a high potassium concentration and a low sodium concentration compared to the fluid outside of the cell. An increase in voltage is called depolarization, and a decrease is called hyperpolarization.

An action potential or "spike" is the signal typically sent from one neuron to another. When a neuron is depolarized to a certain threshold level, voltage-gated sodium channels open and the voltage shoots up very quickly as the positive ions rush into the cell. However, as the voltage climbs, the channels shut again and voltage-gated potassium channels open. These channels cause potassium to rush out of the cell, which hyperpolarizes the membrane even below the resting level, after which it is restored to equilibrium. This entire process is very fast, on the timescale of about 1 ms. Action potentials are sent down the axon of a neuron, and when they reach the end (terminal) of the axon, the high voltage causes the release of neurotransmitter from the axon terminal onto receptors in a dendrite of another neuron. These receptors bind the chemical neurotransmitter and activate ion channels, allowing depolarizing or hyperpolarizing current into the cell. Such a meeting point between one cell's axon and another cell's dendrite is called a synapse. If there are enough depolarizing dendritic inputs, this so-called "post-synaptic" cell will reach spiking threshold and generate an action potential that will be sent to other cells, and so on. There are many exceptions to this description, but this is the most common and therefore canonical way that neurons communicate with each other.

Of course, when one looks closer, the reality of this process is a lot more complicated than this. For one, neurons possess many more kinds of ion channels than just these types of voltage-gated sodium and potassium channels. One example that I will focus on extensively in this thesis is the high-voltage activated calcium channel, a voltage-gated channel that

allows calcium ions into the cell and causes much longer-lasting depolarizations than the spikes of a sodium-mediated action potential.

In addition, given the broad set of complex tasks the brain must execute, there are many different types of neurons with unique physical structures, electrical properties, and functional purposes. I will be focusing specifically on one brain region, the neocortex, and one cell type within this region, the layer 5 pyramidal cell. The neocortex is the outer layer of the cerebrum, the folded layer that features most prominently in any drawing of a brain. The neocortex has many subregions devoted to different tasks including visual processing, motor planning, and language production, but it is characterized by an anatomically conserved laminar structure. Across the neocortex you can observe the canonical six-layer structure, each layer containing different cell types and connectivity profiles. Most neocortical neurons are pyramidal cells, which are characterized by their very long "apical" dendrite, and sub-classified by the layer in which their cell bodies are. Layer 5 pyramidal cells have their cell bodies in layer 5 and dendrites that stretch all the way up to layer 1 (the outermost layer), as well as basal dendrites that extend below the cell body. Accordingly, they are very large (about 2000 µm [1]), and because they span all layers of neocortex, they can receive inputs along the cell from many different sources (Figure 1.1).

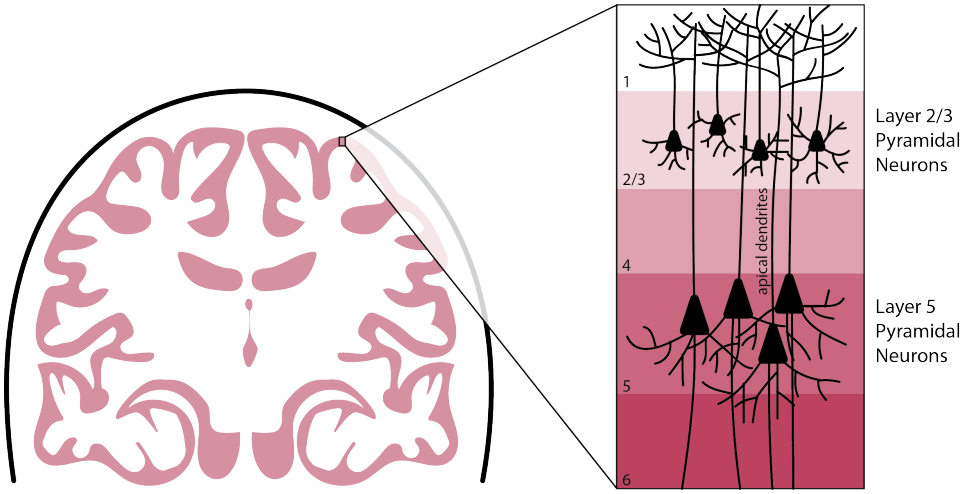

Figure 1.1: Schematic of human neocortex. The diagram shows a cartoon cross section of the brain. The outermost, folded layer (pink) is neocortex, made up of six layers. The magnified version shows how pyramidal neurons are shaped and situated within this laminar structure.

1.2 Recording electrical brain activity

Because neurons communicate electrically, neuroscientists have developed many techniques to record these electrical signals across various spatial and temporal scales. Each has its own advantages and limitations which determine the settings in which they are most useful. They fall into two categories: invasive techniques which require electrodes to be inserted into brain tissue, and noninvasive techniques which can be used without any instruments entering the body. I will give an overview of the main recording techniques to provide an

understanding of the signals I am modeling and how the experimental data I have used to assess my results were obtained.

1.2.1 Invasive techniques

The most direct way to record electrical neural activity is to insert a recording electrode directly into a neuron, producing an intracellular recording. *In vitro*, one can evoke electrical activity using pharmacological agents or by clamping the neuron, either injecting current and recording the voltage changes or fixing the voltage and recording the resulting currents (the latter may seem unintuitive, but it is useful for studying the voltage-gated ion channels I discussed earlier). Because the brain itself does not have pain receptors, electrodes can also be used to record *in vivo*, after an initial surgery under anesthesia to expose the brain tissue. This allows one to directly record electrical events that are generated by actual stimuli in the real world, and also allows one to stimulate a subject and then observe the subject's reaction to this. There are many types of electrodes made for different levels of precision, including multi-electrode arrays for recording signals from many neurons at once.

There are also invasive recordings of neural activity measured over a larger spatial scale. The local field potential (LFP) is a signal recorded by an electrode in the extracellular space of neurons rather from inside the cells. When neurons are active, ions flow into neurons from the extracellular space and vice versa, so the extracellular space is a good place to record activity-dependent electrical activity from all of the cells in the immediate region, up to hundreds of microns. Another technique, electrocorticography (ECoG), uses electrodes placed directly on the surface of the brain to record the electrical activity of the area below. These electrodes have spatial resolution on the scale of millimeters [2]. ECoG has applications in severe epilepsy treatment and brain-computer interfaces in humans [3, 4], as well as research applications in other animals like rats [5].

1.2.2 EEG and MEG

Electroencephalography (EEG) and magnetoencephalography (MEG) are two noninvasive recording techniques for studying electrical brain activity with good temporal resolution [6]. EEG is a widely used recording method where electrodes are placed on top of the scalp rather than inside the skull. MEG is a very similar technique that uses magnetometers to record the magnetic fields induced by the electrical current in the brain, as opposed to the electrodes used in EEG. MEG recordings require much more specialized equipment and experimental settings, but they have the advantage of having better spatial resolution because magnetic fields are less distorted by the skull and scalp than electrical activity [7]. Because they are so far removed from the brain, the signals recorded by EEG and MEG are generated by synchronized activity from tens of thousands of pyramidal cells, and referred to as "macroscale" recordings [6].

While invasive methods are only used in humans under very extraordinary circumstances, such as if they are undergoing neurosurgical intervention for epilepsy and have consented ahead of time [8], EEG only requires the placement of electrodes on the subject's head with conductive gel, so it can be used in pretty much anyone. As a result, a wealth of human EEG data has been collected by clinicians and researchers, and a patient can easily

and painlessly get an EEG done to look for biomarkers of a certain disorder. The downside is that because a single sensor records activity from thousands of neurons, it is very difficult to look at features of the EEG signal and determine the precise neural activity that has generated it. Indeed it is an ill-posed problem, but solving it would enable us to understand how EEG/MEG signals relate to brain function and to develop new treatments based on abnormalities in these signals, which arise in many pathologies.

EEG and MEG signals are generated by the same electrical currents, which are from cortical pyramidal neurons. Pyramidal cells in a given area are all oriented in the same direction, so when many of them exhibit similar electrical activity, the currents travelling up and down the apical dendrites sum (primary current, J^p) and are strong enough to induce secondary volume currents (J^v) and magnetic fields detectable by EEG and MEG sensors outside of the head (Figure 1.2) [6]. Producing a spatial map from EEG or MEG sensor signals to "source-localized" currents J^p in different cortical areas within the brain is referred to as finding an inverse solution. Although finding the inverse solution is an ill-posed problem, there are techniques which impose constraints in order to provide a likely solution, such as minimum-norm estimation and sparse source estimation [6]. The output of these methods is an equivalent current dipole at different locations in the neocortex, measured in units of current $\times$ distance [6]. This is illustrated in Figure 1.2 below.

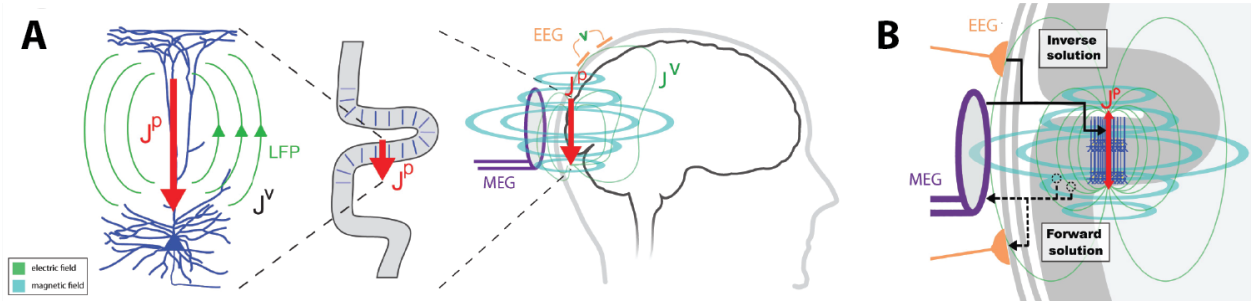

Figure 1.2: Generation of EEG and MEG signals. Figure from Neymotin et al., 2020 [6]. (**A**) Primary currents (J^p) are generated along the dendrites of pyramidal neurons, which are always aligned normal to the cortical surface. These primary currents induce volume currents (J^v) and magnetic fields, which are recorded by EEG and MEG, respectively. (**B**) Inverse solution methods infer the primary currents in cortex (the equivalent current dipole) from EEG or MEG signals, while forward solution methods do the opposite.

However, even after applying an inverse solution method to obtain a source-localized dipole signal, it is unclear how this signal relates to intracellular voltages, spiking, and spiking activity in a neural network. This localized signal is still produced by tens of thousands of cells. To provide some insight in interpreting the cellular and network origin of EEG and MEG signals, the Jones Lab has approached this by developing a computational model of neocortex that can simulate electrical activity in the cells in response to given stimuli and the source-localized EEG signal (dipole) that would result from this. I will cover the neural model in more depth in section 1.4.

1.3 Modeling electrical brain activity

The brain is a large system that is structurally and functionally complex at all scales from molecular to behavioral, so there are many approaches to modeling the brain depending on one's needs or research questions. I will focus specifically on the use of differential equations to model a neuron's voltage and transmembrane electrical currents as a function of its inputs and its biophysical properties.

1.3.1 The Hodgkin-Huxley model

In a 1952 paper, authors Alan Hodgkin and Andrew Huxley derived a system of four differential equations to model a neuron's voltage based on electrophysiological experiments performed on squid neurons, specifically the giant axon that runs down the squid's body [9]. This description of the voltage changes in an axon using electrical circuit theory earned the authors the 1963 Nobel Prize in Physiology or Medicine and laid the groundwork for many efforts in computational neuroscience [10]. The Jones Lab model that I have worked with is more complex, but is built on the same ideas and forms of equations, and because the scale of the Hodgkin-Huxley model is much more tractable, it is worth discussing in some detail to provide a sense of how these models work. Part of what makes this model simpler is that it disregards the shape of the cell, effectively approximating the neuron as a single point.

The Hodgkin-Huxley model accounts for three types of ionic currents: fast voltage-gated sodium currents, delayed-rectifier voltage-gated potassium currents, and "leak" currents which describe ions being channeled and pumped across the membrane to maintain its resting potential at around -65 mV [11]. The opening and closing of any single ion channel is stochastic, but because there are so many sodium channels in the membrane, one can deterministically model the proportion of sodium channels that are open at any given time with a good degree of accuracy. As discussed, opening and closing channels causes transmembrane currents and thus changes the cell's voltage.

The four differential equations describe the change in the following variables over time:

- V - membrane voltage
- n - proportion of potassium gates open
- m - proportion of sodium gates activated
- h - proportion of sodium gates deinactivated

The variables m, n, and h are called gating variables because they describe the molecular "gates" that open and close membrane ion channels in a voltage-dependent manner. The sodium channel requires two gating variables because it has an activation gate and an inactivation gate, which leads to the confusing terminology that a sodium channel is either activated or deactivated and either inactivated or deinactivated at any given time. Both gates must be open on a channel for the ion to pass through (in other words, the channel must be activated and deinactivated). The leak current does not require a gating variable because it is not gated by voltage.

Each of the gating variables are described by equations of this form:

$$\frac{dn}{dt} = \alpha_n(V)(1-n) - \beta_n(V)n \tag{1.1}$$

Here $\alpha_n(V)$ is the rate at which potassium channels open as a function of voltage, and $\beta_n(V)$ is the rate at which they close as a function of voltage, with both functions being nonnegative for all $V \in \mathbb{R}$, such that when m is initialized in [0,1] (as it would be in all real settings, since m is a proportion), it stays in this interval, as desired.

Dividing through by $\alpha_n(V) + \beta_n(V)$, this can be rewritten as

$$\tau_n(V)\frac{dn}{dt} = n_\infty(V) - n \tag{1.2}$$

Here, $\tau_n \doteq \frac{1}{\alpha_n(V)+\beta_n(V)}$ and $n_\infty(V) \doteq \frac{\alpha_n(V)}{\alpha_n(V)+\beta_n(V)}$. This form is useful because it says that the proportion of open channels tends toward a steady state value $n_\infty(V)$, at a rate of $1/\tau_n$. We can then draw n_∞ and τ_n as functions of V to get a sense of what happens to the potassium channels at different voltages (Figure 1.3).

The m and h equations are defined in exactly the same way, except that their α and β functions have different forms. Figure 1.3 shows the steady states and time constants of each gate as functions of the membrane voltage, V, for a typical choice of parameters. As you can see, sodium channels activate rapidly (τ_m is small) as voltage increases, with potassium channels following more slowly. However, as voltage climbs, sodium channels begin to become inactivated ($h_\infty = 0$, so these gates close). When the voltage decreases again, sodium channels deactivate and potassium channels close again (m_∞ and n_∞ decrease). However, sodium channels also slowly deinactivate ($h_\infty > 0$ but τ_h is large), so they can open up the next time the activation gates open.

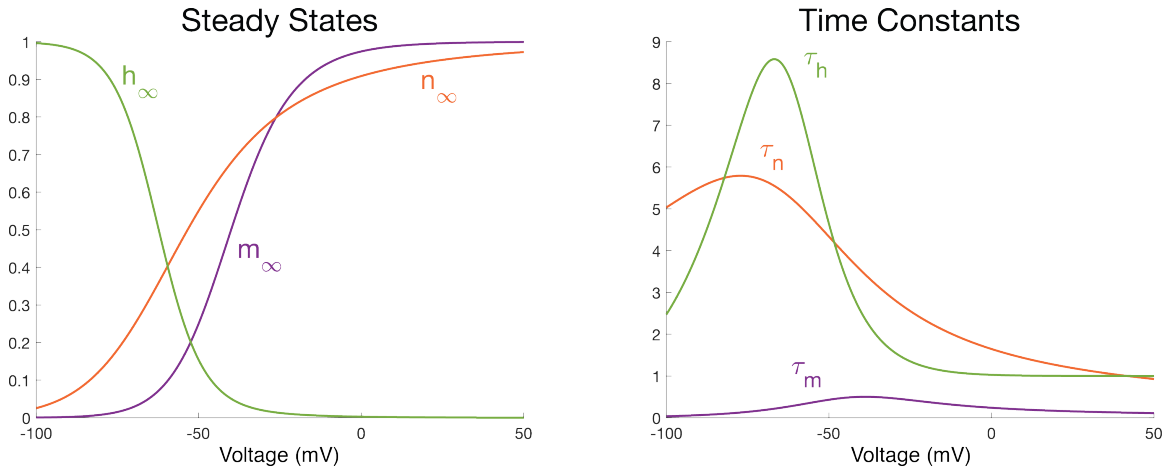

Figure 1.3: Steady state values and time constants of Hodgkin-Huxley gates. The graph on the left shows the steady-state values of m (purple), n (orange), and h (green), which describes the proportion that would be open at the given voltage as $t \to \infty$. The graph on the right shows the time constants of each of these gates as functions of the membrane voltage, where smaller τ values correspond to faster change.

The last piece of the system we must define is the equation for $\frac{dV}{dt}$ as a function of m, n, and h, as well as the input current $I(t)$, which could be from a synaptic connection or from an experimenter's manipulation. The voltage changes according to the following equation, which I will explain term by term [12].

$$C\frac{dV}{dt} = \bar{g}_{\text{Na}}m^3h(E_{\text{Na}} - V) + \bar{g}_{\text{K}}n^4(E_{\text{K}} - V) + \bar{g}_{\text{leak}}(E_{\text{leak}} - V) + I(t) \tag{1.3}$$

C is the (constant) capacitance of the membrane, so that the entire equation is of the form $C\frac{dV}{dt} = \sum I$, if $\sum I$ denotes the net transmembrane current. In other words, the capacitive current is equal to the sum of the transmembrane ionic currents.

The next three terms are all scaled by a constant parameter $\bar{g}_{\text{ion}}$, which is the maximum conductance for that current. From a biological perspective, this can be interpreted as the number of ion channels in the membrane per unit area. For example, in real neurons $\bar{g}_{\text{Na}}$ is much greater than $\bar{g}_{\text{leak}}$, so when sodium channels open they cause very large currents compared to the leak current.

These same three terms also all contain a factor of the form $E_{\text{ion}} - V$. E_{ion} is defined as the "reversal potential" for that current. If all other currents were ignored, each ionic current would cause the membrane voltage to go towards their value of E_{ion}, at which point due to concentration and electrical gradients there would be no net current into or out of the cell. Thus the factor $E_{\text{ion}} - V$ pulls the voltage towards the equilibrium value at a rate proportionate to how far it already is from this value.

For the leak current, the underlying cellular mechanisms are approximately constant under all conditions, so its maximum conductance and the disparity between the current voltage and its equilibrium voltage are enough to completely characterize its contribution to the cell's voltage. However, for the two voltage-gated channels, we must take into account whether the channels are open or closed, which is where our gating variables come in. Because there are multiple subunits in ion channels, each of which contain their own independent gates, some of the gating variables are raised to exponents (although these exponents were chosen by Hodgkin and Huxley to fit the data, not because they knew the structure of these channels) [11]. This means the proportion of open delayed-rectifier potassium *gates* open is n, but the proportion of open delayed-rectifier potassium *channels* is only n^4.

In summary, the voltage is determined by the input current and contributions of each ionic current, which are determined by that channel's density $\bar{g}$, the reversal potential E, and the proportion of open channels as determined by any gating variables.

For a typical set of parameters, there are three types of behaviors that can be evoked by a constant input current. A hyperpolarizing current or a weak depolarizing current will not evoke any spiking because the input will not push the voltage far enough above its resting value to cause m gates to open. A stronger excitatory current will open the m gates and cause the cell to spike, returning afterwards to a slightly higher equilibrium value. With still stronger input current, the model cell will enter a state in which it continuously spikes at regular intervals. These three behaviors are shown in Figure 1.4.

In Figure 1.4 I have also provided a phase plane visualization of the system showing $V(t)$ plotted against each of the gate variables $m(t)$, $n(t)$, and $h(t)$. As shown, these values are barely perturbed from their steady state values in the subthreshold case before returning to a stable equilibrium. The one spike case also corresponds to an equilibrium point solution

for each of these gate variables, which is approached after the initial input knocks these values onto a cyclical trajectory back to this point. In contrast, a strong input current results in a system with no equilibrium point. In this case, the system enters a limit cycle, which is why the neuron continues to spike at regular intervals.

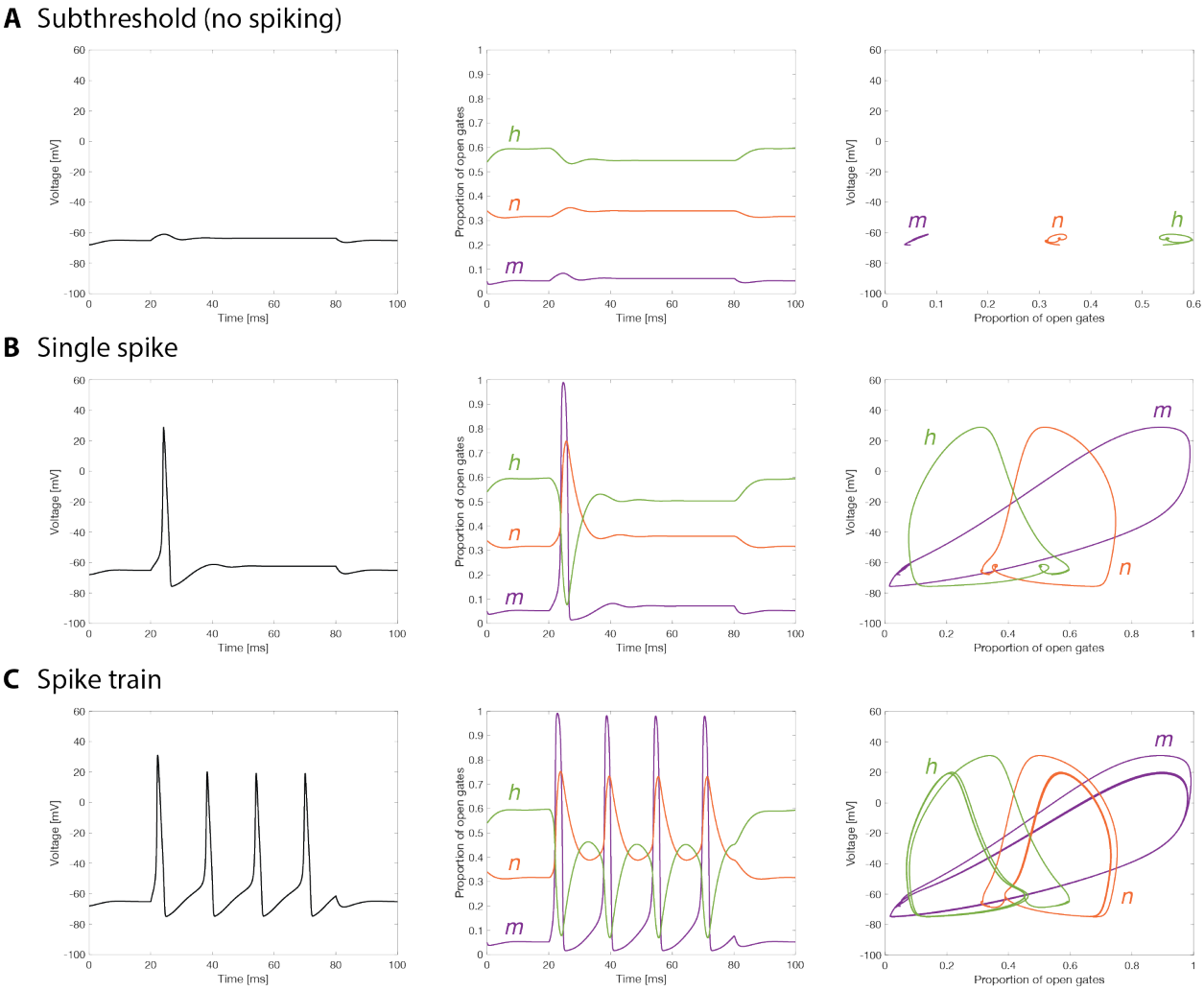

Figure 1.4: Solutions to the Hodgkin-Huxley equations for different levels of input current. In all three simulations, $I(t)$ was set to a positive constant for 20-80 ms, and 0 everywhere else. Plots on the left show voltage traces (voltage $V(t)$) versus time, middle plots show the three gating variables plotted against time, and plots on the right show phase planes with $V(t)$ on the y-axis against the three gating variables on the x-axis. (**A**) $I(t) = 2$ nA slightly depolarizes the neuron but does not result in spiking. (**B**) $I(t) = 4$ nA is only strong enough to evoke one spike. (**C**) $I(t) = 10$ nA is strong enough to evoke a train of spikes at regular intervals.

There are many parameters in this system and it is highly nonlinear, which makes it very difficult to solve analytically. However, this makes it a useful model because it allows the model, whose parameters were originally calculated from the giant axon of a squid and have biophysical interpretability, to be used to approximate the behavior of many neuron types across species and brain regions. It also provides a template one can use to customize

the set of ionic currents included in the model. For example, if one wants to add chloride ionic currents, they can extend the so-called Hodgkin-Huxley formalism to include gating variables for these channels, then add another term to the voltage equation that raises these variables to the relevant exponents and scales by $\bar{g}_{\mathrm{Cl}}(E_{\mathrm{Cl}} - V)$. This increases accuracy and often allows for more types of behavior from the model neuron (for example, a set of several spikes which die out and do not create a continuous oscillation for the duration of the input). As I will discuss, the Jones Lab takes advantage of this versatility by adding many more types of currents including potassium M-currents, hyperpolarization-activated cation currents, and the current in which I am most interested, the calcium current through L-type channels.

1.3.2 Compartmental model neurons

The Hodgkin-Huxley model was a scientific breakthrough, but you may have found it odd that the previous section completely disregarded dendrites, axons, and synapses. Indeed, as mentioned above, in the classic formulation, Hodgkin-Huxley neurons are "point neurons." This means that all of the ionic currents and the resulting voltage changes are modeled as occurring in a single point in space. Thinking back, it is clear that point neurons are unable to capture some important aspects of the problem at hand, such as the fact that EEG signals are dominated by current flowing up and down pyramidal neuron dendrites, and that layer 5 pyramidal cells are important because their long shape allows for inputs from all other layers to arrive at different points along the membrane.

One solution, established by Wilfrid Rall, is to model the neuron not as a point, but as a cylinder (one-dimensional cable) or a system of connected cylinders, each of which is specified by its length, diameter, and various resistance and capacitance quantities [13, 14, 15]. Transmembrane currents are still modeled according to Hodgkin-Huxley type equations, but they are introduced at a certain point along the cable. From there, current flow through the cylinder(s) is modeled according to cable theory.

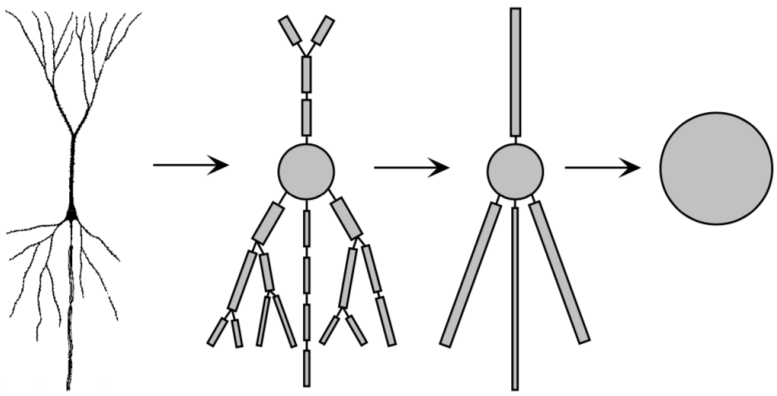

Figure 1.5: Schematic showing compartmental model neurons in decreasing complexity. This figure, taken from Dayan and Abbott's *Theoretical Neuroscience* [11], shows a real pyramidal cell at left, followed by a series of possible compartmental models of this neuron using fewer and fewer compartments.

If neurons did not have voltage-gated ion channels along their dendrites, post-synaptic electrical signals arriving in the dendrites would still change as they propagated toward the soma due to cable properties or "passive membrane" properties of the cell (as opposed to "active membrane" properties from ion channels, which are accounted for by Hodgkin and Huxley). These electrical properties include the cell's membrane resistance per unit area R_m, membrane capacitance per unit area C_m, and internal resistance of the cell R_i, as well as morphological properties like a dendrite's length and diameter.

In this framework, the change in voltage along the cell can be calculated using the cable equation, which can be stated as

$$\lambda^2 \frac{\partial^2 V}{\partial x^2} = V + \tau \frac{\partial V}{\partial t} + I(V, x, t) \tag{1.4}$$

Here, x is position along the cable, t is time, V is the difference between the membrane voltage and the resting potential ($E_{\text{rest}} - V_{\text{membrane}}$), and λ and τ are constants called the time constant and the length constant, respectively [15]. I is the function that accounts for inputs and active membrane properties.

More precisely, τ is a decay term which can be thought of describing how fast the voltage decays back to rest after a current (or, more generally, how quickly the voltage responds to a voltage change). This is easier to see when you imagine that F and $\frac{\partial^2 V}{\partial x^2}$ are set to zero, meaning that the whole cable is at the same voltage and there are no membrane currents. In this case, the cable equation can be expressed as $\frac{\partial V}{\partial t} = -\frac{V}{\tau}$, a simple ordinary differential equation solved by $V(t) = Ce^{-t/\tau}$. It is defined as $\tau = R_m C_m$. Since the value of C_m is fairly constant across neurons, it effectively only depends on R_m for the cell. Similarly, λ is a decay term across space, describing how much an electrical signal attenuates as it propagates further down the cable, away from the source of the current. It is defined by $\lambda = \sqrt{\frac{rR_m}{2R_i}}$, where r is the radius of the cable's circular cross section [15].

In practice, the partial differential equation usually is not actually solved along each cylinder. Instead, as Rall himself did, it can be approximated by dividing the cylinder into discrete segments, then reducing the problem to a system of ordinary differential equations [16]. These equations are of the form

$$c_j \frac{dV_j}{dt} = \frac{I_{\text{input}}}{A_j} + I_{\text{ion}} + \sum_k g_{j,k}(V_k - V_j) \tag{1.5}$$

where c_j is the membrane capacitance of neuron j, A_j is the surface area of neuron j, $g_{j,k}$ is the conductance from segment k to segment j, I_{input} is input current, and I_{ion} is ionic current, a way of abbreviating all of the gating variable terms described in section 1.3 [11, 17]. The constant $g_{j,k}$ is equal to 0 if segments j and k are not connected, and if they are connected, it is equal to

$$g_{j,k} = \frac{r_j r_k^2}{R_i L_j (L_j r_k^2 + L_k r_j^2)} \tag{1.6}$$

where R_i is intracellular resistance, L_j is the length of segment j, and r_j is the radius of segment j [11].

With the power of computation, this paradigm can be used on a scale from Rall's single "equivalent cylinder" [16] to highly detailed neuronal reconstructions with hundreds of compartments [18]. Because this cable model is so powerful, simulation environments have been designed to make it relatively easy to construct these models by allowing users to instantiate objects like compartments and electrodes according to their locations and attributes without having to set everything up from scratch and write code to solve the cable equations. One such simulation environment, NEURON [17, 19], is used to create the Jones Lab's model.

1.4 The Jones Lab model

The Jones Lab models a canonical neocortical circuit designed to simulate source-localized EEG/MEG signals (i.e, primary current dipoles, see J^P in Figure 1.2). The model contains four cell types: layer 2/3 pyramidal cells, layer 5 pyramidal cells, layer 2/3 basket cells, and layer 5 basket cells. A schematic of the model is shown in Figure 1.6.

I introduced pyramidal neurons in section 1.1 above, and they are described in greater detail below. Another important type of neuron is the basket cell. These cells form inhibitory synapses directly onto the soma of a nearby pyramidal cell. Unlike pyramidal cells, their dendritic projections are very short and typically aligned radially around the soma. This means that the electrical activity in the dendrites of basket cells tends to cancel out when summed, so basket cells do not directly contribute to the EEG signal, although the effects of their inhibition on the network are very important. For these reasons, they are modeled as point neurons with only a single compartment 39 µm in length and 20 µm in diameter. They only contain the classic Hodgkin-Huxley sodium, potassium, and leak channels, with the following parameters tuned to reproduce the fast spiking dynamics characteristic of this cell type: $R_a = 200\,\Omega\cdot\text{cm}$; $C_m = 85\,\mu\text{F/cm}^2$; $\bar{g}_{\text{Na}} = 0.12$ S/cm^2; $\bar{g}_{\text{K}} = 0.036$ S/cm^2; $\bar{g}_{\text{L}} = 0.003$ S/cm^2; $E_{\text{Na}} = 50$ mV; $E_{\text{K}} = 77$ mV; $E_{\text{L}} = 54.3$ mV [20].

The two pyramidal cell types are modeled in greater biophysical detail in order to accurately account for the dendritic currents that generate the primary current dipole signal. Their morphologies are based on a 1993 paper by Bush and Sejnowski, in which an elaborate 400-compartment model was systematically reduced to the fewest possible compartments while still retaining accurate electrical properties, including the longitudinal current flow between compartments [21]. This reduction is practical because it allows simulations with hundreds of cells to be done in a reasonable amount of time.

The L2/3 pyramidal cells are comprised of eight compartments. The morphology and dimensions of these compartments are shown in Figure 1.6. In addition to sodium, potassium, and leak channels, they contain adapting potassium currents (also called muscarinic potassium or M-currents) [22]. The L5 pyramidal cells are comprised of nine compartments, with on extra compartment in the apical dendrite (see Figure 1.6). In addition to the currents contained in the L2/3 cells, they contain L-type (fast) calcium currents, T-type (slow) calcium current, potassium-activated calcium currents, and hyperpolarization-activated currents (H-currents). The morphology and dimensions of these cells are shown in Figure 1.6A and 1.4B, respectively.

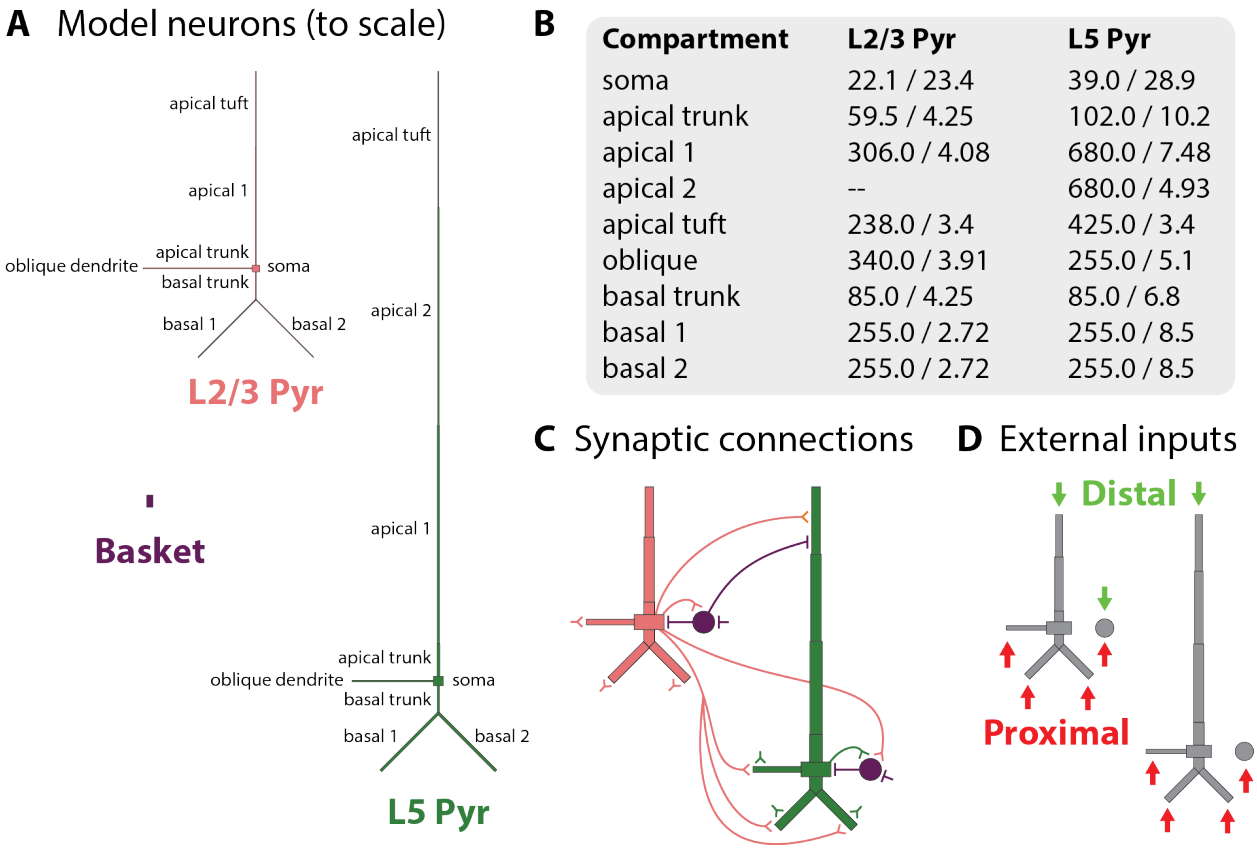

Compartment	L2/3 Pyr	L5 Pyr
soma	22.1 / 23.4	39.0 / 28.9
apical trunk	59.5 / 4.25	102.0 / 10.2
apical 1	306.0 / 4.08	680.0 / 7.48
apical 2	--	680.0 / 4.93
apical tuft	238.0 / 3.4	425.0 / 3.4
oblique	340.0 / 3.91	255.0 / 5.1
basal trunk	85.0 / 4.25	85.0 / 6.8
basal 1	255.0 / 2.72	255.0 / 8.5
basal 2	255.0 / 2.72	255.0 / 8.5

Figure 1.6: Jones lab model network. (**A**) To-scale depiction of the different cell types in the model, with each compartment labeled with its name. (**B**) Table describing the length / diameter parameters for each compartment (in μm). (**C**) Schematic of the local synaptic architecture. Y-shaped synapses are excitatory and T-shaped synapses are inhibitory. Disembodied synapses represent connections from other cells of the same type. (**D**) Schematic showing compartments that receive exogenous inputs from proximal (red) and distal (green) drives in the model.

The arrangement of these four cell types is based on the canonical structure of neocortex. L5 basket cells inhibit the somas of L5 pyramidal cells, and L2/3 basket cells inhibit the somas of L2/3 pyramidal cells as well the apical tufts of L5 pyramidal cells. L2/3 pyramidal cells form excitatory synapses onto the basal and oblique dendrites of other L2/3 pyramidal cells and L5 pyramidal cells, as well as onto the apical tufts of L5 pyramidal cells and onto L2/3 basket cells. L5 pyramidal cells only form excitatory synapses onto the basal and oblique dendrites of other L5 pyramidal cells and onto L5 basket cells.

A synapse in this model is a way of connecting the spiking output of one neuron to the input current $I(t)$ of another. Without explicitly modeling axons, we can model a synapse between neuron i and neuron j by taking each time point that neuron i spikes (defined as the somatic voltage crossing a certain threshold), creating a double exponential shaped current starting at this time point, and adding it to the $I(t)$ term of neuron j in the specified compartment. In this model there are two types of excitatory synapses, AMPA and NMDA, and two types of inhibitory synapses, GABA_A and GABA_B. These are only differentiated by their rise and decay times as well as the fact that inhibitory synapses have a flipped sign. It

is also possible to adjust the synaptic strength, which is the maximal conductance factor by which to multiply this current, as well as the synaptic delay, which is a time shift between the presynaptic cell's spike and the input current to the postsynaptic cell (meant to account for time spent travelling along the axon).

The user can specify the size of this model by entering the dimensions of a grid of these cell types. For example, a 10×10 grid would give 100 of each cell type, each connected to the other cell types as outlined in the above paragraph. To make the model more realistic, the strengths of the connections between pairs of cells are inversely related to the distance between them, so that cells are most strongly coupled to the neighboring cells. Similarly, cells that are far apart will have longer synaptic delays. The space constants that govern these relationships can be found in Jones et al., 2009 [22].

Importantly, there are several ways to provide inputs to this model, which are necessary to generate activity and to represent a simulation experiment that mimics an empirical experiment. One way is to apply tonic current to one or more of the cell types, akin to what would be done in a classical intracellular electrophysiology. These currents are applied directly into the cells and are specified by their start and endpoints as well as their strength (nA). While useful in some research applicants, this tonic applied current does not reflect the type of inputs that a cortical region would be receiving in a real brain while EEG or MEG is being recorded.

There are two main pathways of input to the cortex that relay information from other parts of the brain to a local cortical circuit. Thus, the model also provides two input pathways, named "proximal" and "distal" according to the location of the post-synaptic effects on the proximal (close to soma) and distal (far from soma) dendrites of the pyramidal neurons (Figure 1.6D). In practice, the user simulates trains of action potentials that activate synapses on the pyramidal and basket cells in the locations shown in Figure 1.6D (in exactly the same way that they receive synaptic inputs from the other model cells). These proximal and distal inputs or "drives" are essential for approximating real activity from a cortical network. The proximal input pathway represents feedforward input from thalamus, a brain region that receives most sensory inputs before the neocortex does. The distal input pathway simulates feedback input from other regions of neocortex or from nonspecific thalamic nuclei, which project to upper layers of the cortex. When using the Jones lab model, the user can define as many input patterns as they like, each with different strengths and temporal profiles. The synaptic strength (maximal conductance) of these inputs can also be tuned individually for each cell type. This means that, for example, I can create a proximal input that does not affect the layer 2/3 cells, despite them being included in this pathway, by changing the synaptic strength to 0 for these connections. There is one other type of input provided in this model, which is a noisy Poisson synaptic input to the somas of the neurons, with a strength and frequency that can be specified for each cell type.

The last step is to compute the source-localized primary current dipole signal from the electrical current generated inside the model neurons. This is done by taking the intracellular currents in a pyramidal neuron's dendrites and summing the components that run parallel to the axis of the apical dendrite, then multiplying by the length of the dendrite (see Figure 1.2) [22]. Summing this quantity across the entire pyramidal neuron population (layer 2/3 and layer 5) gives the simulated primary current dipole signal. The result has units of current $\times$ distance (nAm), so it is directly comparable to source-localized recorded EEG/MEG data.

As you can see from Figure 1.6A, the layer 5 pyramidal neurons have much longer dendrites than the layer 2/3 pyramidal neurons, so currents from these layer 5 cells contribute much more substantially to the dipole than the layer 2/3 cells do.

This model is built with the NEURON Python simulation environment. The source code is made up of Python files as well as NMODL files (a NEURON-specific descriptive programming language), which mathematically define ion channel kinetics and other functions such as computation of the dipole and the LFP generated by the network. The Jones Lab has built a graphical user interface around this model and made it available as a software package called Human Neocortical Neurosolver (HNN, https://hnn.brown.edu), which is what I used for the work in this thesis, though I did make local changes to the underlying code to modify the model and expand the recording and plotting capabilities of the simulations. More detailed descriptions of the model and software can be found in [20, 22, 6].

This model has been used by the lab to propose network-level neural mechanisms by which commonly measured EEG signals such as evoked responses and low frequency oscillations are generated [20, 22, 23, 24]. I have been expanding it to improve the calcium dynamics in the model and to investigate the impact of calcium events in layer 5 pyramidal cells on human EEG/MEG signals. Calcium dynamics have not previously been studied in detail in the Jones Lab model.

Chapter 2

Improved Calcium Model

2.1 Calcium spikes

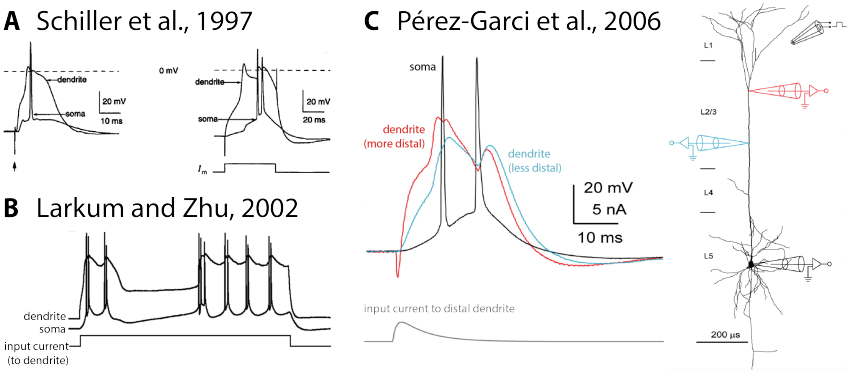

Figure 2.1: Examples of dendritic calcium spikes in electrophysiological recordings in vitro. All plots show simultaneous voltage traces recorded both the soma and apical dendrite of a layer 5 pyramidal neuron. (**A**) Left: distal synaptic stimulation leads to a dendritic calcium spike. Right: current injection into the apical dendrite ($800\,\mu\text{m}$ from the soma) leads to a dendritic calcium spike. Results in rat cortex. [25] (**B**) Continuous current leads to dendritic calcium events that cause "bursts" of somatic action potentials. Results in rat cortex. [26] (**C**) Left: double exponential shaped input to the distal dendrite leads to a calcium spike which attenuates slightly as it moves toward the soma but still creates a two-spike burst. Right: setup of stimulating and recording electrodes, which is very similar to the setup for the figures displayed in (A) and (B) as well. Results in mouse cortex. [27]

I began Chapter 1 by describing the action potential, a sharp depolarization event which arises from the influx of sodium through voltage-gated channels, and I showed simulated action potentials generated by solving the Hodgkin-Huxley equations. This is not the only type of nonlinear electrical event that occurs in neurons. Pyramidal cells also contain several types of voltage-gated calcium channels, which can cause a different type of depolarization event called a calcium spike. Calcium spikes are broader, longer depolarizations. Significantly, they often occur in the apical dendrites of these neurons, in some cases being unaccompanied by an action potential at the soma [25, 28]. These events are primarily caused by the opening of L-type calcium channels, which open rapidly and stay open for a relatively long time, and are considered "high voltage activated" compared to

other voltage-gated calcium channels like the T-type channel (also included in the model) [29]. The long depolarization that occurs during a calcium spike often generates one or more sodium/potassium spikes in the soma on top of the calcium event, which is referred to as a calcium burst (examples from real neurons shown in Figure 2.1).

We were very interested in the influence of these non-synaptic electrical events on the network activity and the EEG readout. In particular, it seemed that dendriticly-generated calcium spikes that do not reach the soma because they have attenuated or been blocked by inhibition should produce a large signature in the dipole.

Our interest was bolstered by a 2017 paper entitled "Dendritic calcium spikes are clearly detectable at the cortical surface" [30]. The authors, Mototaka Suzuki and Matthew Larkum, used surface electrode arrays (similar to ECoG) in rats to record activity on the cortical surface. They found that optogenetically evoked calcium spikes in anesthetized rats as well as sensory evoked calcium spikes in awake rats were visible in their surface electrode recordings. To confirm that these were indeed calcium spikes, they used pharmacological techniques (including blocking synapses with CNQX and applying the $GABA_B$ agonist baclofen in order to downregulate calcium channels) as well as laminar electrodes, which were able to confirm the current sink was occurring in the apical dendrite of layer 5 pyramidal neurons. Some of the main results are summarized in Figure 2.2 below.

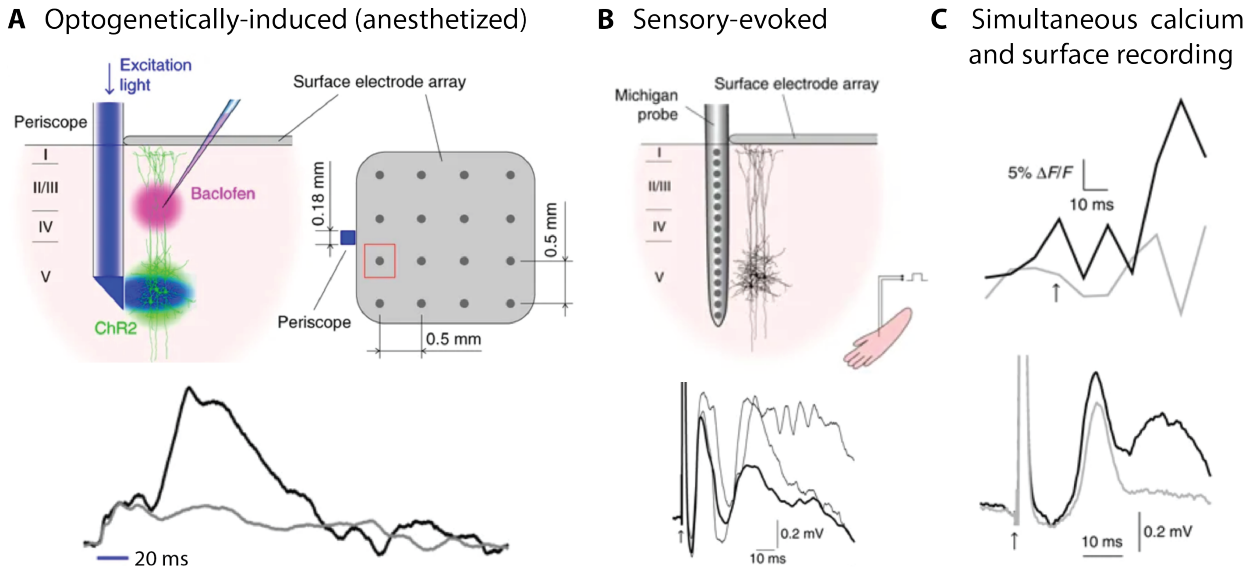

Figure 2.2: Summary of main findings in Suzuki and Larkum, 2017 [30]. (**A**) The experimental setup for evoking calcium spikes in layer 5 neurons by driving back-propagating action potentials in the soma. Below is the average surface electrode recording in the presence of a putative dendritic calcium spike (black) compared to lack of spike (grey). (**B**) The experimental setup for recording during hindpaw stimulation. The illustration shows the hindpaw being stimulated while the relevant area of cortex is being recorded both with a surface electrode and with a Michigan probe, which records extracellular voltage changes at many cortical depths. Below is the average surface electrode recording (thick) as well as two examples of traces where a particularly large late event emerged (thin). (**C**) Simultaneously recorded calcium transients (top) and surface potentials (bottom). In both plots, black and grey lines are the average over 20 measurements with and without putative calcium spike, respectively.

This work prompted us to turn to our own lab's model to see whether or not it is likely that we would see similar results in humans. The concept was simple: just as Suzuki and Larkum did experimentally, we would drive the layer 5 pyramidal cells to produce dendritic calcium spikes, then observe what the output dipole would look like and how it related to the cellular and network activity, with potentially exciting implications for the interpretation of human EEG signals. However, once I started to do this, we realized our model was not faithfully reproducing the calcium dynamics that have been shown in layer 5 cells in electrophysiology work. In light of this, I took on the task of adjusting the model cells to improve the fit to experimental data.

2.2 Retuning the electrical properties of layer 5 pyramidal cells

2.2.1 Problems with existing model

Different types of neurons exhibit different spiking patterns, as a result of their morphologies and ionic conductances. The layer 5 pyramidal cell model previously used in the Jones Lab and currently distributed with the HNN modeling software were tuned to produce "intrinsic bursting" behavior [20]. When a constant current is applied, an intrinsic bursting cell will produce "bursts" of several action potentials which are extremely close together in time (Figure 2.3). This is as opposed to a regular spiking cell, which will produce single action potentials at a fairly regular frequency, which increases as the input current gets stronger (Figure 2.3). You may recall that the classic Hodgkin-Huxley model generates regular spiking behavior. Layer 2/3 pyramidal cells are typically regular spiking cells, while layer 5 pyramidal cells are often intrinsically bursting cells (though both types exists; see section 2.3.1) [31]. The pyramidal cells in the Jones Lab models were tuned to reflect this qualitative distinctions between the two layers.

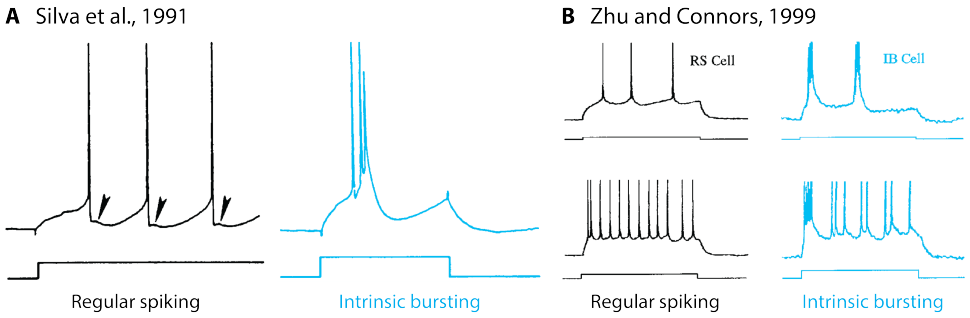

Figure 2.3: Comparison of regular spiking and intrinsic bursting. (**A**) A layer 2/3 regular spiking cell (left, black) compared to a layer 5 intrinsic bursting cell (right, cyan). Results from mouse neocortex *in vitro* [31]. (**B**) Another example of a regular spiking cell (left, black) compared to an intrinsic bursting cell (right, cyan). In this case, two levels of current were applied to show how both cells respond to a stronger level of activation. Results from anesthetized rat neocortex *in vivo* (specifically barrel cortex, similar to somatosensory cortex in humans) [32].

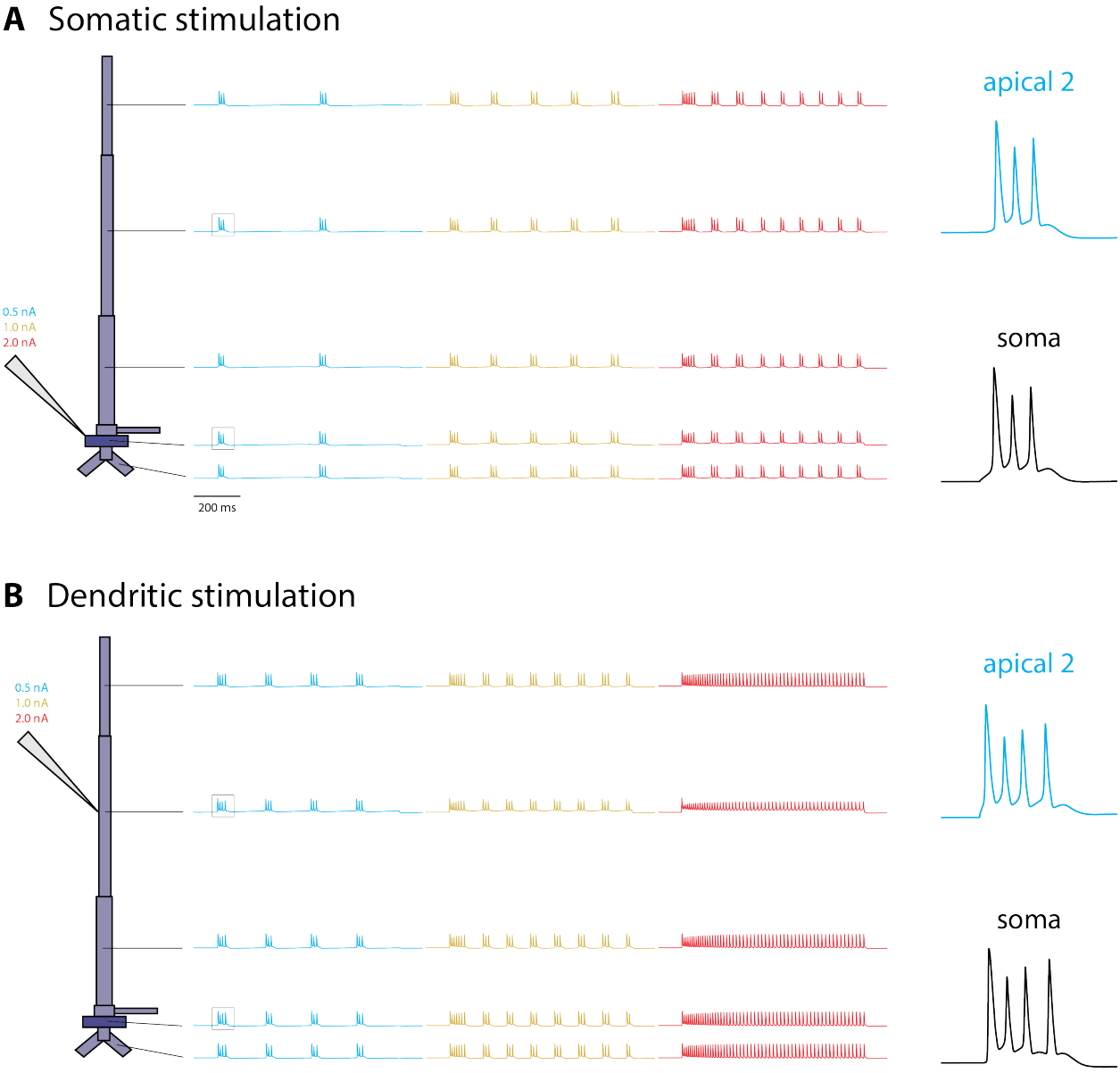

Figure 2.4: Model layer 5 pyramidal neuron's response to simulated current injection. In both panels, voltage traces are shown from five compartments: apical tuft, apical 2, apical 1, soma, and basal 2, in order from top to bottom. Simulations are 1000 ms long, with current applied from 100-900 ms. In each, three strengths of current are applied: 0.5 nA (blue, left), 1.0 nA (yellow, middle), and 2.0 nA (red, right). Boxes indicated the portions of the trace that are magnified at right to provide more detail. (**A**) Model current clamp applied to the soma. (**B**) Model current clamp applied to apical 2. Notice that the strong (2.0 nA) input pushes the neuron out of its intrinsic bursting into a state of runaway excitation which persists until the stimulus offset.

However, the cells were only tuned to replicate electrophysiological data at the soma. In order to do this research, I had to write code to produce plots of calcium concentration, calcium current, and voltage in several compartments throughout the layer 5 pyramidal neuron, in addition to the somatic voltage plots that were already included in the model. After doing this and looking at the electrical properties of the distal dendrite, it was clear

that the model results did not reflect the properties of real dendrites, as observed in the whole cell recordings, e.g. Figure 2.1.

Figure 2.4 shows the result of isolating a single model layer 5 pyramidal neuron and simulating constant current injection. As you can see, both somatic and dendritic stimulation evoke narrow, pointy spikes in all compartments of the cell. It is clear that the difference in electrical properties between the dendrites and the soma, namely that there are sodium/potassium spikes riding on top of the calcium spike in the soma but not in the dendrite (as seen in Figure 2.1), is not being preserved in the model. Therefore, we are not able to get anything that matches the data and looks like a canonical calcium spike.

This was a significant problem for trying to understand calcium spikes using our model. It would not make much sense to use our model output to make claims about dendritic calcium spikes if the dendritic voltage traces in our model were not reflective of experimental recordings of these events. Beyond the question of calcium spikes, it was also an opportunity to improve the accuracy of the model in reproducing other features of experimentally observed pyramidal neuron dynamics. It was impossible to know what we were missing or getting wrong in our simulations without making this change. Much of my third chapter will be devoted to expanding beyond the particulars of calcium spikes to investigating the way in which calcium affects the dipole signal in response to fairly simple input patterns. In the remainder of this chapter, I will discuss several approaches I took to try to adjust the model to improve fit to electrophysiological data recorded from layer 5 pyramidal dendrites, while preserving the somatic response, and end by showing how the improved model compares to the old model and the real neuronal recordings.

2.2.2 First approach: adjusting calcium conductances

The default layer 5 pyramidal cell model includes L-type calcium currents (Ca), T-type calcium currents (CaT) which are hyperpolarization-activated, and potassium-activated calcium currents (KCa). For each current, the value of the conductance per unit area ($\bar{g}$) in the soma is a parameter, which makes it easy to manipulate without changing the underlying model. The same is true for the conductance per unit area in the dendrite. This means that just within the space of changes that can be made by only adjusting parameters as the user, there are already six continuous variables which directly affect the flow of calcium into the cell. As a starting point, I tested whether manipulating the conductance of each of these calcium currents could account for the discrepancies in the shape of calcium events in the dendrite.

After sweeping through biologically realistic values of these conductances (data not shown), I was unable to improve the accuracy of the dendritic voltage traces. This meant that there was something more fundamentally missing from the layer 5 pyramidal neuron model, which would require changes to its underlying structure and biophysics.

2.2.3 Second approach: accounting for calcium diffusion

The second approach I considered and tested was to make the model of calcium ions in the cell more sophisticated. Moreso than most of the other ions involved in the transmembrane currents I have been describing, calcium has many complex effects on the cell's functioning.

Calcium ions function as signalling molecules or second messengers in many biochemical pathways inside the cell. They can also be stored and released by the endoplasmic reticulum of a neuron, and undergo a buffering reaction inside the cell of the form $\mathrm{CaB}^{2+} \rightleftharpoons \mathrm{Ca}^{2+} + \mathrm{B}$, where B represents a generic buffer (not boron) [33]. Furthermore, the Jones Lab model accounts for calcium flow across the membrane and voltage flow between compartments, but it does not actually model calcium ions diffusing through the compartment and the cell. All of these factors affect the intracellular calcium concentration in different regions of the cell, which should affect the electrical output.

We started with implementing calcium ion diffusion throughout the compartment and down the length of the dendrite. Our motivations for trying this went beyond attempting to improve the voltage traces in the dendrite. A former postdoc, Dr. Robert Law, with whom I worked closely when I joined the Jones Lab, was interested in the flow of calcium into the soma (and possibly building up there) during a dendritic spike. We thought that dynamics like this could be important for the realism of the calcium spike model, and for the ultimate computations that the cell could perform such as aiding in plasticity and learning.

When researching this approach I looked to other models of neuronal calcium dynamics. The first was a 1985 paper by Fogelson and Zucker [34]. This model compares a one-dimensional model of calcium diffusion away from the membrane and a three-dimensional model of the same phenomenon. The idea is based on the diffusion equation, which is $\frac{\partial u}{\partial t} = D\frac{\partial^2 u}{\partial x}$ in the one-dimensional case. Their model also includes a calcium pump which removes calcium from the cell at a constant rate P [34, 35]. Since our pyramidal cells are so long and narrow, I thought the one-dimensional model should suffice and would be much less computationally expensive than a two- or three-dimensional model of calcium diffusion.

I also looked closely at a 1993 paper by Nowycky and Pinter which modeled calcium diffusion and buffering [36]. In this model, the cell was spherical, and the diffusion equation was modeled as a system of ordinary differential equations, one for each concentric "shell." Each equation was of the form:

$$\frac{d[S]_i}{dt} = \frac{D_S}{V_i \delta}(A_{i-1}([S]_{i-1} - [S]_i) - A_i([S]_i - [S]_{i+1})) \tag{2.1}$$

"where $[S]_i$ is the concentration of diffusible species [...], D_S is the diffusion coefficient, δ is the shell thickness, and V_i is the shell volume. A_{i-1} and A_i are, respectively, the surface areas of the outer and inner spherical boundaries of the i^{th} shell" [36]. I felt this could be applicable to the pyramidal cell model, but with cylindrical segments down the length of the dendrite rather than spherical shells. The analogous equation I generated to describe this was the following:

$$\frac{d[\mathrm{Ca}^{2+}]_i}{dt} = \frac{D_{\mathrm{Ca}}}{r_i^2 h_i^2}\left(r_{i-1}^2([\mathrm{Ca}^{2+}]_{i-1} - [\mathrm{Ca}^{2+}]_i) - r_i^2([\mathrm{Ca}^{2+}]_i - [\mathrm{Ca}^{2+}]_{i+1})\right) \tag{2.2}$$

where $[\mathrm{Ca}^{2+}]_i$ is the intracelllular calcium concentration in segment i, r_i is the radius of segment i, h is the height of segment i, and D_{Ca} is the calcium diffusion coefficient. The value of this coefficient was set to $2 \times 10^{-}6$ cm^2/s in this paper [36] and to $6 \times 10^{-}6$ cm^2/s in Zucker's work [35, 34].

The trickier part was implementation. My first thought was that these equations could be written into the NMODL files that described the intracellular calcium concentration

in the cells. However, it was proving difficult to integrate this with the many other ionic mechanisms in the cell. I found out that NEURON has a reaction-diffusion (rxd) module which could be imported into our model since it is built using NEURON [37]. This allows the user to define substances that undergo chemical reactions or diffusion throughout the cell. With the generous help of Dr. Robert McDougal at Yale University, who helped to create this module, I was able to use the rxd package to allow calcium to diffuse throughout the cell, as well as a pump (in place of the old calcium decay mechanism), as in Zucker's model [35].

Unfortunately, this also was unable to account for the lack of broader dendritic depolarizations. I looked to the literature to test different plausible values of the diffusion coefficient for calcium [38, 39, 40], and I also tried different ways of defining the region over which calcium diffused within the neuron. However, none improved the model accuracy. Some paradigms produced similar results as the regular model, while some introduced very strange spiking behavior, like a single spike followed by a long, flat depolarization in the soma. None were able to produce bursts of thin spikes in the soma accompanied by broad spikes in the dendrite, which is what I was looking for.

This led me to more thoroughly review the literature for other computational models that were used to simulate dendritic calcium activity in layer 5 pyramidal cells, in order to figure out what was going wrong with my calcium model. I came to the conclusion that calcium diffusion and buffering were not required to model dendritic calcium spikes, but that the distribution of ion channels throughout the cells may need to be altered beyond what could be achieved by feeding in different parameters for the somatic and dendritic values.

2.2.4 Final approach: redistributing dendritic ion channels

The first paper I tried adapting to the Jones Lab model was a 2015 paper by Shai et al., where they used a detailed compartmental model of a mouse layer 5 pyramidal neuron to model calcium spikes and bursting [41]. Modifying the channel densities to match the parameters in their paper produced very unrealistic results, but when I instead changed the parameter values to match the relative ratios in the dendrite versus the soma it started looking better. However, the first spike of the burst was still too narrow and pointy in the dendrite.

I had better success when I turned to a 2014 paper by Almog and Korngreen to look at their conductance parameters [42]. The authors of this paper used a genetic algorithm to optimize the electrical properties of a layer 5 pyramidal neuron to fit their dataset of current clamp recordings. This work was highly relevant because they were looking specifically at dendritic spikes, and they paid special attention to the role of calcium channels in their optimization process. First, they did not include calcium currents and tuned all other parameters to fit a dataset with calcium channel blockers applied. Then, they included the calcium channels back in and ran the optimization process again, tuning the calcium parameters while constraining the other parameters not to deviate too far from their previous values. One important difference from our model was that rather than just having one conductance parameter in the soma and another in the dendrite for each current, they defined continuous functions along the dendrite to allow conductances (or, analogously, density of ion channels in the membrane) to change gradually. They constrained their potassium channel densities to be exponential decay functions, and their sodium and calcium densities to be

linear functions which leveled off at some point along the dendrite. The parameters of these functions, such as the slope and the start and end values, were tuned in the optimization process.

I applied this setup to the Jones Lab model, adapting the underlying code of the model to allow the dendritic ionic conductances to change continuously as a function of distance from the soma, rather than being constrained to a single value. Then, I used their optimal values to begin hand tuning the distributions. Initially, I had trouble preserving the intrinsic bursting behavior as opposed to the regular spiking behavior, but eventually I found a set that produced bursting in the soma in a manner similar to the original Jones Lab model, but with the dendritic voltage traces looking much more similar to experimental data (i.e. lower, broader depolarizations in the distal dendrites, Figure 2.5).

I was able to narrow it down to three important conductances, which, perhaps unsurprisingly, were sodium, voltage-gated potassium, and fast (L-type) calcium. In the tuning process, I had also applied this framework to other currents, such as M-type potassium, T-type calcium, and potassium-activated calcium, but I found I was able to revert these back to the original values and still produce the broad dendritic spiking and somatic bursting that I was looking for. The sodium conductance decreased linearly through the dendrite before plateauing in the distal dendrite, the calcium conductance increased linearly before plateauing in the distal dendrite, and the potassium conductance decreased exponentially throughout the dendrite (see Figure 2.5C and Table 1). It is worth mentioning that this increased calcium conductance in the dendrite was inconsistant with the Almog and Korngreen paper, which found a decreasing calcium conductance with distance [42], but it was consistent with the Shai et al. paper I discussed earlier [41]. There is also experimental support for increased calcium conductance and decreased potassium conductance in the distal dendrites [43, 44]. In the final step of tuning, I also ensured that the network spiking behavior was similar to that of the original model in a simulation of an event-related potential, a canonical EEG feature (event-related potentials and network activity will be discussed in Chapter 3).

L5 Pyr cell parameter	Jones 2009	Improved model
Soma Kv channel density (S/cm^2)	0.01	0.06
Soma Na channel density (S/cm^2)	0.16	0.32
Soma Ca channel density (S/cm^2)	60	10
Dendrite Kv channel density (S/cm^2)	0.01	0.0001
Exponential decay coefficient		-0.006
Dendrite Na channel density (S/cm^2)	0.14	0.0028
Plateau point (μm)		962
Dendrite Ca channel density (S/cm^2)	60	40
Plateau point (μm)		1501

Table 1: Parameter changes made to layer 5 pyramidal cells. The "plateau point" refers to the distance from the soma at which the conductance levels out at the dendritic value, as opposed to linearly approaching that value as a function of the distance (see Figure 2.5). Dendritic Kv channel density value is interpreted as a vertical shift in the exponential decay function. All other parameters were unchanged from the existing model [22].

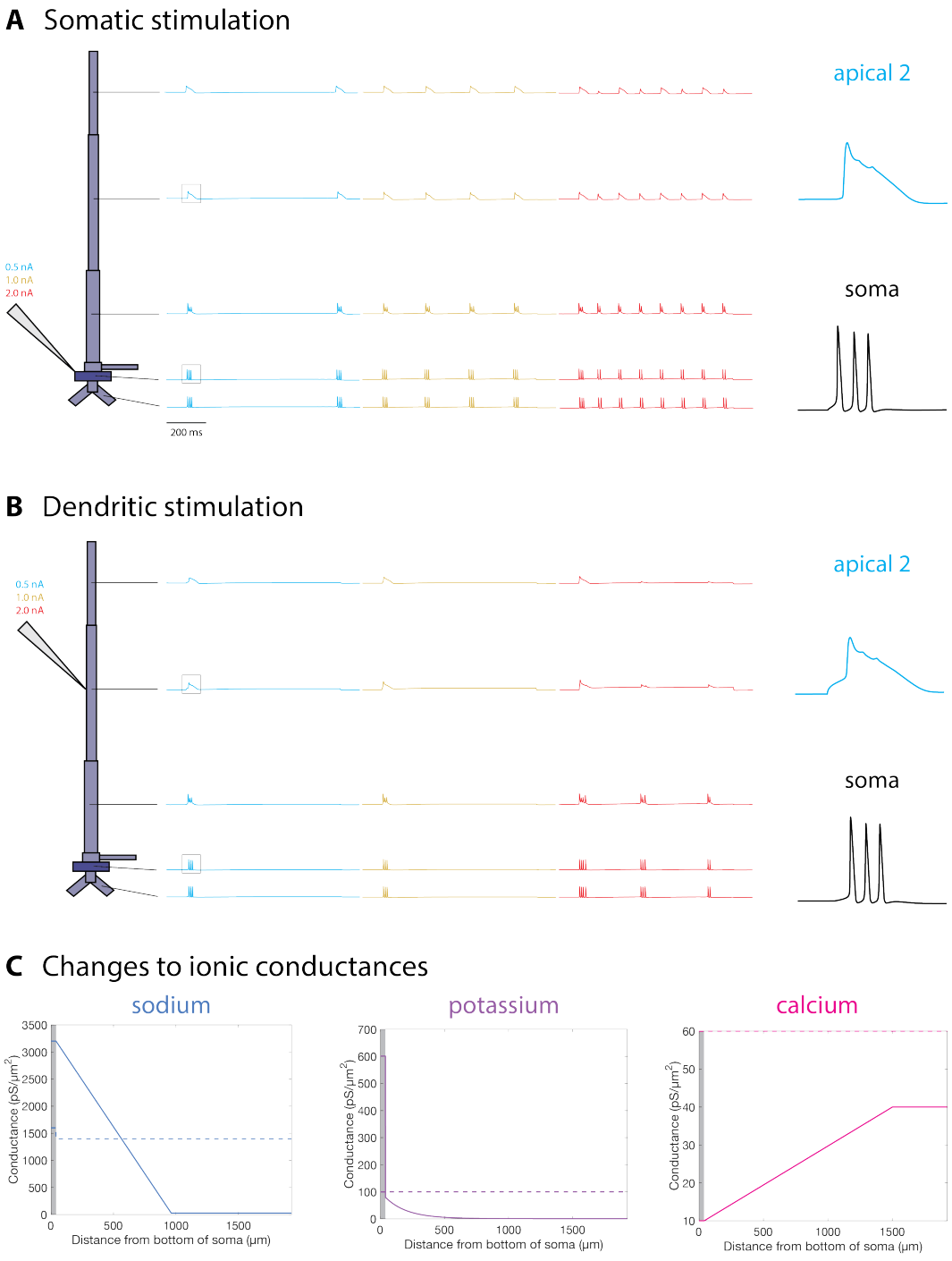

Figure 2.5: New model layer 5 pyramidal neuron's response to simulated current injection. Panels A and B are directly analogous to Figure 2.4., showing the voltage traces from each of the five indicated compartments at 0.5 nA, 1.0 nA, and 2.0 nA currents. (**A**) Model current clamp applied to the soma. (**B**) Model current clamp applied to apical 2. (**C**) The conductances of sodium, voltage-gated potassium, and fast calcium currents are each shown as a function of distance from the bottom of the soma (with the shaded region being the soma itself). Dotted lines indicate the Jones 2009 model, and solid lines indicate the new model I have tuned to produce more accurate dendritic voltage traces.

Overall, this made the dendrite more electrically passive and toned down the classic Hodgkin-Huxley conductances that produced that narrow spike. Also, making this change continuous, rather than an immediate change between the soma and dendrite, allowed the soma and the dendrite to have the qualitatively different behaviors they need to have to replicate electrophysiological findings. By this, I meant that if the sodium was dropped immediately to a much lower value by simply changing the dendritic conductance parameter (not the model itself), the soma would not behave properly because the soma and the apical trunk are too closely connected.

In Figure 2.5, I show the behavior of the final model. Notice that this qualitatively retains the somatic spiking in response to somatic excitation while broadening the spike width in the dendrites. It also eliminates the unrealistic runaway excitation in the presence of strong dendritic input.

2.3 Comparison to experimental results

2.3.1 General results

Overall, the updated model provided a better fit to the experimental data than the original model. Figure 2.6 provides a summary of this result, showing the voltage traces from the model neurons compared to experimental data recorded from rodent neurons.

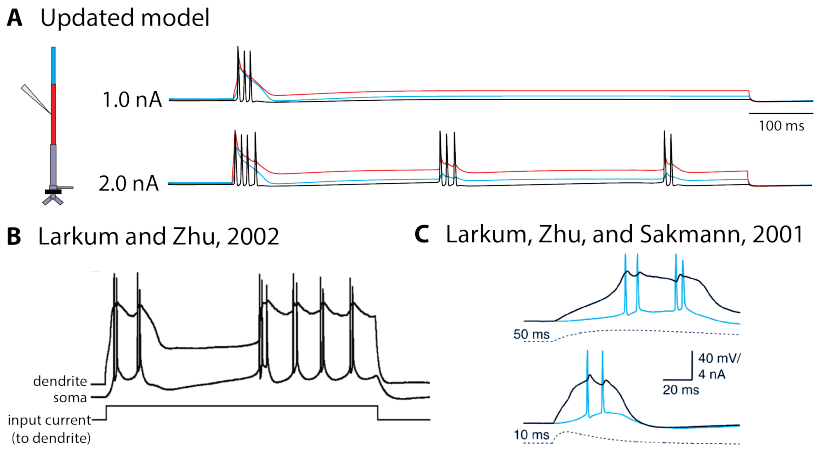

Figure 2.6: Updated model improves fit to in vitro electrophysiology data. (**A**) Model with current applied to apical 2. Voltage traces from the tuft, apical 2, and the soma are overlaid, with trace colors corresponding to the compartment colors at left. (**B**) Experimental data from dendritic applied current in rat neocortex (also shown in Figure 2.1). [26] (**C**) Dendritic (dark blue) and somatic (light blue) responses to current applied to the distal dendrite in rat neocortex. The dotted lines show the shape of applied current. [45]

One behavior that my model did not replicate was the finding that backpropagating action potentials in the soma may need to reach a "critical frequency" to evoke a calcium spikes. The phenomenon has been reported in several articles, and is shown in Figure 2.7 [46, 47]. In my model, calcium spikes were achieved whenever a somatic burst was evoked. However, after dwelling on this for a bit, I concluded that it made sense that this would not

happen in our intrinsic bursting cells because the evoked spikes are always at a fixed within-burst frequency of about 100 Hz. Layer 5 neurons in rodent cortex can be either bursting or regular spiking, which may account for this discrepancy–data showing the critical frequency phenomenon must be taken from regular spiking cells because these cells are capable of displaying spikes at a range of frequencies (see Figure 2.7) [48, 49]. On the other hand, while intrinsic bursting cells display varying levels of activity in response to different inputs, this tends to be reflected in decreasing latency between burst events rather than increasing frequency within the spikes in a single burst. It could be interesting to include both cell types in the Jones Lab model in the future.

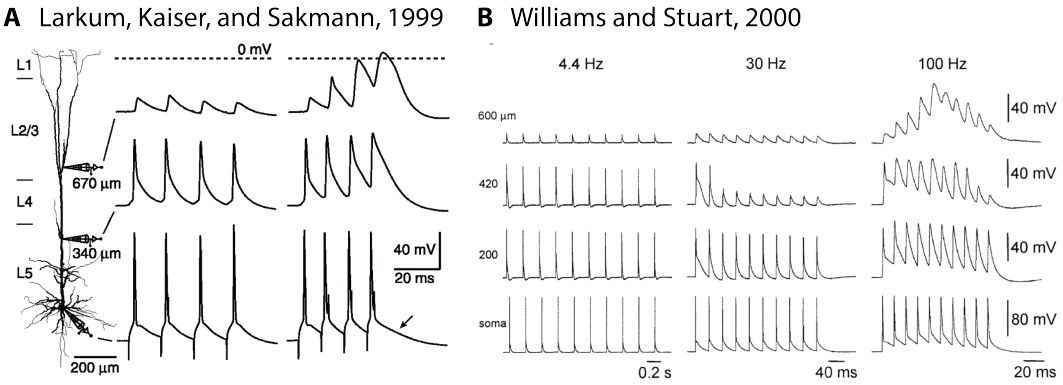

Figure 2.7: A critical frequency of somatic action potentials evokes dendritic calcium influx in regular spiking layer 5 cells. Both examples are from rat neocortex in response to rhythmic stimulation. [46, 47]

2.3.2 Calcium spikes in surface recordings

Our original motivation for looking at calcium activity in the layer 5 cells was to see if the finding that dendritic calcium spikes are visible in surface electrode recordings in rats would translate to our model of human EEG signals. To create a similar stimulation paradigm as their optogenetics experiment, I generated a strong proximal input that only applied to the layer 5 pyramidal neurons. The spikes in this stimulus were distributed with a mean at 40 ms and a standard deviation of 5 ms, such that almost all spikes occured in the 30-50 ms window. In addition, I also created a mock "baclofen" condition to compare to this condition in the experimental paper [30]. Baclofen is an agonist of $GABA_B$ receptors, meaning that it binds to these receptors and fools them into thinking they have received $GABA_B$ from a presynaptic inhibitory cell. This results in hyperpolarizing current wherever baclofen is applied. Our model does not have a clear way to activate postsynaptic receptors in the absence of a presynaptic spikes, like can be achieved with pharmacology, so in my version, which I refer to as the $GABA_B$ condition, I created noisy "Poisson" inputs to layer 2/3 basket cells to drive this inhibition of the layer 5 pyramidal cells' distal dendrites. To make this condition more similar to the baclofen condition, I changed the location of the synapse to the apical 2 compartment (not the apical tuft) and changed the synapse type from $GABA_A$ to $GABA_B$.

Because our model output is actually source-localized EEG data (primary current dipole signal) and not sensor-level EEG data, it was not directly comparable to the surface

electrode data (voltage at the surface). In light of this, we decided to instead look at the voltage traces in the apical tufts of these cells, since electrodes on the surface of the head would mostly be picking up on these layer 1 electrical events. I averaged the tuft traces among all of the 100 layer 5 pyramidal cells in the network, since surface electrodes record from a group of cells rather than just one (layer 2/3 pyramidal cells were excluded because they were not activated in this simulation). This is still not a perfect approximation of what surface potentials actually measure, which is obvious by the order of magnitude difference between our results and Suzuki and Larkum's (scale bars in Figure 2.8A and Bii), but it is enough to know if we are on the right track.

Proximal input ("optogenetics")	
Start time mean (ms)	40
Start time standard deviation (ms)	5
Number of spikes per input	1
L2/3 Pyr AMPA weight (μS)	0.0
L2/3 Pyr NMDA weight (μS)	0.0
L2/3 Basket AMPA weight (μS)	0.0
L2/3 Basket NMDA weight (μS)	0.0
L5 Pyr AMPA weight (μS)	1.0
L5 Pyr NMDA weight (μS)	0.0
L5 Basket AMPA weight (μS)	0.0
L5 Basket NMDA weight (μS)	0.0

Poisson input to L2/3 Basket ("baclofen")	
L2/3 Basket AMPA weight (μS)	10.0
L2/3 Basket NMDA weight (μS)	0.0
L2/3 Basket frequency (Hz)	80.0
L2/3 Basket → L5 Pyr weight (μS)	0.0

Table 2: Inputs used to approximate experiments from Suzuki and Larkum, 2017 [30]. Poisson inputs were provided exclusively to L2/3 Basket cells for the duration of the 150 ms simulation. Besides increasing the L2/3 Basket *to* L5 Pyr synaptic weight, I also changed the type of synapse from $GABA_A$ to $GABA_B$ and changed the location of the synapse from the apical tuft to apical 2.

These average tuft voltages looked strikingly similar to the experimental surface electrode data (compare surface potential in Figure 2.8A to Figure 2.8Bii). In particular, the proximal input meant to simulate optogenetic drive provoked a significant and sustained peak in the simulated surface potential. This peak was significantly reduced by turning off the L-type calcium conductances to prevent calcium spiking, and it was completely flattened in the $GABA_B$ condition (Figure 2.8Bii).

In Figure 2.8B I also provide other model data to give more insight on the network activity. I show the current dipole output for each of these simulations (Figure 2.8Biii). Interestingly, in the proximal input paradigm (the control condition (black), as compared to the no Ca^{2+} and $GABA_B$ conditions), the current dipole signal shows a significant negative deflection, while in the other two conditions the overall waveform is positive. This pattern will be discussed further in Chapter 3. I have also included comparisons of the calcium concentrations in each compartment in both the control and $GABA_B$ conditions (Figure 2.8Biv). The dendritic calcium activity that backpropagates from the proximal input site is abruptly cut off in the apical 2 compartment by the strong $GABA_B$ connection. Calcium does not enter this compartment nor the tuft above it.

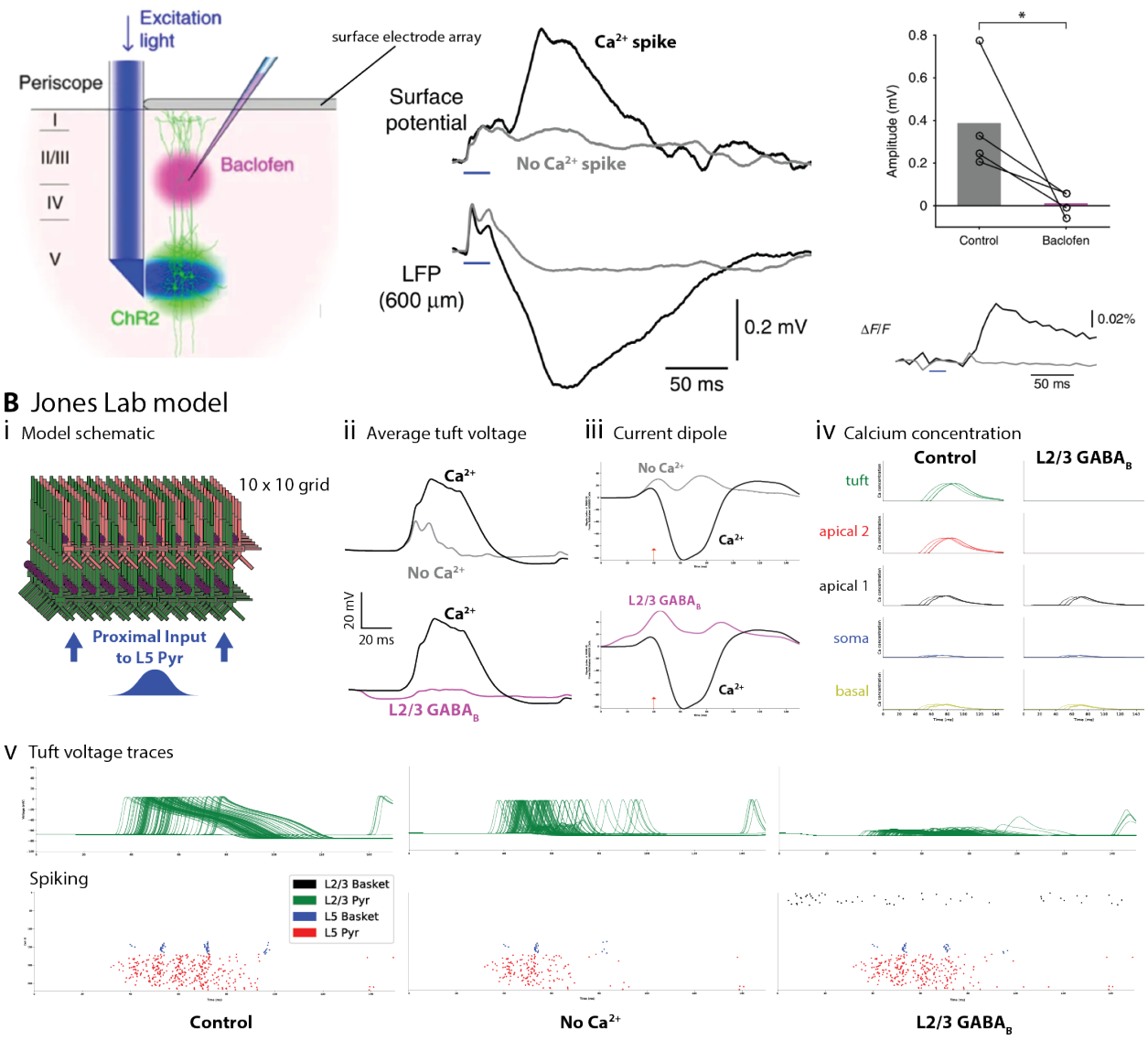

Figure 2.8: Calcium spikes in the updated model. (**A**) Results from Suzuki and Larkum, 2017 provided for reference [30]. On the left is their experimental setup for optogenetically-induced calcium spikes. At center are average surface electrode and LFP recordings in the presence and absence of a putative Ca^{2+} spike. At right is a graph showing that the this peak amplitude was drastically reduced by the presence of the $GABA_B$ agonist baclofen, as well as a depiction of calcium indicator fluorescence change over time. (**B**) Results from my modeling work in the Jones Lab model. **i** Schematic showing the network and simulation. **ii** Averaged apical tuft voltage traces for a single simulation the input. Grey trace shows results when L-type calcium conductances are set to 0 in all compartments and pink trace shows the condition with strong $GABA_B$ inhibition in the apical dendrite (described in text). **iii** Current dipole corresponding to the simulations in panel ii. **iv** Calcium concentration in compartments along the primary axis of the cell in the control (Ca^{2+}) condition and the $GABA_B$ condition. **v** More data on these three simulation conditions. At the top are all of the tuft voltage traces in each condition, which can be compared to their averages in panel ii. At the bottom are the raster plots in each condition.

Finally, I have shown the individual voltage traces (green) in the tufts of each layer 5 pyramidal neuron in the three conditions, as well as the raster plot in each of these three conditions (Figure 2.8v). Raster plots display each somatic action potential as a dot on a graph with time on the x-axis and individual cells along the y-axis. These are interesting to consider because they add more nuance to what is shown in the averaged tuft voltages. It is striking how differently the tuft voltage traces are shaped in each of the three conditions. The control condition shows the long, broad depolarizations that I achieved through my tuning, described in section 2.2. The no Ca^{2+} condition shows significantly thinner, pointy voltage traces as well as significantly reduced overall spiking. Finally, the $GABA_B$ condition shows a good deal of spiking, but the tuft voltages during these spikes are almost flat due to this inhibition.

There are still some ways in which my simulation output does not match the recorded data from Suzuki and Larkum 2017. In my simulations, the calcium-spike-driven peak lasts about 70-80 ms in the averaged tuft voltage, while in their surface electrode data it appears to last about 110-120 ms. There is also a discrepancy in that their peak takes longer to occur from the onset of the light stimulus (shown in blue) than ours does. More broadly, it is clear that this modeling and their experiments and recording methods were not exactly comparable. For example, there are important differences between rats and simulated human responses, and applying optogenetic stimulation and pharmacological agents like baclofen is somewhat different from simulating their effects through model synapses. Nonetheless, the overall qualitative match between my results and theirs is very supportive that the model is accurately capturing the neural dynamics of the brain. Based on this model, the presence of a dendritic calcium spike should be discernible in both surface electrode (ECoG) recordings and source-localized EEG data in humans. I am also confident that this new version of the model is a step in the right direction for realistically simulating the cortical dynamics that underlie EEG biomarkers.

In the next chapter I will deal entirely with the new model and show how fast calcium currents shape the network's response to typical inputs, and how this is reflected in the EEG output.

Chapter 3

Role of Calcium in Stimulus-Evoked EEG Features

3.1 Event-related potentials

One stereotypical EEG feature is the event-related potential (ERP). This is a waveform that is time-locked to an event (for example, a visual, auditory, or tactile stimulus, or a movement by the subject) and usually averaged over many trials. When this averaging is performed on data from the relevant electrode, which will be dependent on the type of event, the ERP has characteristic peaks and troughs, indicating that the underlying neural activity is probably conserved across performances. ERPs are also referred to as evoked responses, as in "auditory evoked response" or "motor evoked response." They can be observed either at the EEG sensor level or at the current source level (i.e. at the level of the dipole, which our model simulates). Differences in ERP features have been used by neuroscientists and clinicians as markers of attention, development, memory, PTSD, dyslexia, and schizophrenia, to name just a few applications [50, 51, 52, 53, 54, 55].

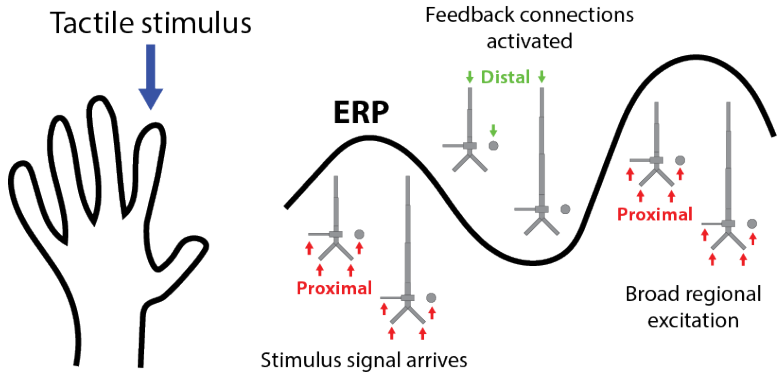

Figure 3.1: ERP schematic. When a tactile stimulus is delivered to the hand, the current dipole response from the hand region of primary somatosensory cortex exhibits an ERP signal with a stereotyped waveform as shown. Using our neocortical model, we hypothesize that this is generated by a sequence of proximal and distal inputs as shown and discussed in the text.

The Jones Lab has studied ERPs, particularly in the context of tactile perception and attention tasks carried out by our lab. Several joint EEG/MEG and modeling studies by our lab have posited that these ERPs in primary somatosensory cortex (the first area of neocortex that tactile input reaches) are caused by time-localized proximal then distal inputs, followed by a strong, broad proximal input [20, 56, 57]. The idea is that the first proximal input is the tactile information first reaching the cortex from the thalamus, which is a relay center for sensory inputs before they disperse throughout cortex for processing. This initial thalamic input comes into the granular layers of the cortex and then hits the proximal dendrites of the pyramidal neurons. The subsequent distal input occurs when that information reenters this area cortex via feedback connections from further processing areas, such as higher order cortex. The later strong, broader proximal input likely reflects re-emergent thalamic input that arises as part of a thalamocoritcal loop of information. A more detailed description of these input parameters is provided in Table 3.

Default ERP Inputs	Proximal 1	Distal 1	Proximal 2
Start time standard deviation (ms)	2.47	3.85	8.33
Number of spikes per input	1	1	1
L2/3 Pyr AMPA weight (μS)	0.01525	0.000007	1.44
L2/3 Pyr NMDA weight (μS)	0	0.0043	0
L2/3 Basket AMPA weight (μS)	0.08831	0.0065	0.000003
L2/3 Basket NMDA weight (μS)	0	0.02	0
L5 Pyr AMPA weight (μS)	0.00865	0.1425	0.684
L5 Pyr NMDA weight (μS)	0	0.08	0
L5 Basket AMPA weight (μS)	0.19934		0.009
L5 Basket NMDA weight (μS)	0		0

Table 3: Evoked input parameters characterizing the default ERP simulation. Red inputs are proximal, green are distal. In the default ERP, the mean time of the inputs is as follows: proximal 1 at 26.61 ms, distal 1 at 63.53 ms, and proximal 2 at 137.12 ms.

Using my new model of the layer 5 pyramidal cells with improved calcium dynamics, I looked at the role that L-type calcium currents play in the response to these ERP-generating inputs. Surprisingly, the generated current dipole response was fairly similar in the control case versus the case where these currents were blocked (by setting the conductance to zero), even though the latter case virtually eliminated spiking from layer 5 pyramidal cells in response to the distal input (red dots in raster plot in Figure 3.2B). The difference in spiking activity in the two conditions mainly occurs between the offset of the first proximal input and the onset of the second proximal input (about 40 ms - 125 ms). The distal input is strong enough to elicit a sizable depolarization in the apical tuft, even without the calcium currents, but the signal attenuates down the dendrite until it is too weak to effect a burst of spikes at the soma unless these active calcium currents are present. Nonetheless, the main electrical event is that of current being pushed down the dendrite, and the spikes seem not to matter once the dipole is smoothed. Dipole smoothing and scaling is applied to the model result in

order to account for averaging effects that occur in real data, which comes from a larger and more heterogenous network than we are simulating. I note that here I have focused only on the current dipole contribution from the layer 5 pyramidal neurons, without discussing the contribution from the layer 2/3 pyramidal neurons. This choice was both because the layer 5 pyramidal cells' longer dendritic length gives them a stronger influence on the net current dipole shown and because the layer 2/3 cells do not include calcium currents.

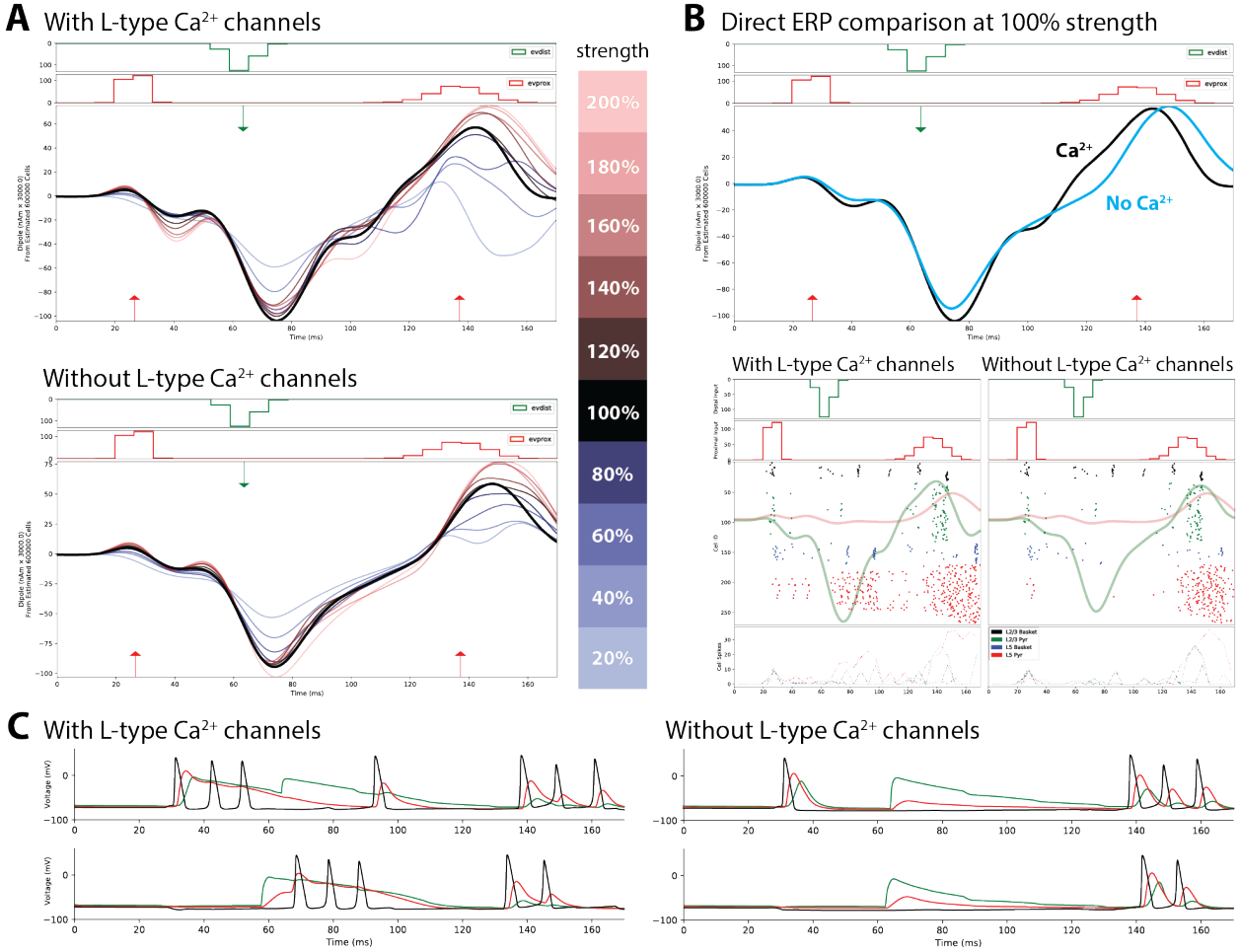

Figure 3.2: L-type calcium currents significantly affect spiking, but not primary current dipole, in response to typical ERP inputs. (**A**) Comparison of ERP with L-type calcium currents and without. The bolded black dipole signals are in response to the default ERP inputs. The thinner red and blue traces show the response when all of the synaptic weights in each of the three inputs are scaled up or down in strength, according to the legend at right. Mean start times of each input were 26.1 ms, 63.53 ms, and 136.12 ms. (**B**) The upper panel overlays the ERPs with and without these calcium channels, which look fairly similar. The lower panel compares the raster plots, showing L2/3 basket cells (black), L2/3 pyramidal cells (green), L5 basket cells (blue), and L5 pyramidal cells (red). Displayed on the same plot as the rasters are primary current dipoles from layer 2/3 (pink) and layer 5 (green) alone, which sum to create the dipoles seen in the other figures. Dipole smooth window is 30 ms in all figures, to better approximate the temporal resolution of averaged EEG data. (**C**) Example voltage traces from layer 5 pyramidal neurons are shown, with recordings from the soma (black), apical 2 (red), and apical tuft (green) from the same neuron overlaid.

From here, it made sense to look at individual inputs to see the effects of these calcium currents, in order to more clearly understand the network's response to different exogenous conditions. In addition to giving me more insight into the generation of ERPs, it also is useful to understand generally how the model network response to simple excitatory drives from the feedforward (proximal) or feedback (distal) input pathways. A systematic characterization of the model response to various types of input provides a framework to help infer the underlying neural generators of various waveform features. Thus, in future studies, the problem of estimating the model parameters that can generate a specific waveform will be better constrained.

3.2 Feedforward excitation

Our lab's model of ERP generation requires two proximal inputs. These are interpreted as feedforward inputs, meaning that they move in the direction from sensory receptors to higher-level processing via the thalamus. Both proximal ERP inputs cause a small upward deflection followed by a sustained trough. In the case of proximal 1, which is weak by comparison, the trough is modest in size, and the response is not much affected by the presence of L-type calcium currents (Figure 3.3A). This is due to the fact that the dipole is dominated by the layer 5 pyramidal cells which do not fire action potentials, since they outnumber those that do by a factor of 24 to 1, and the behavior of these cells is not affected by L-type calcium currents in this case. As you can see from the thin traces, these calcium currents make more of a difference in the stronger inputs, which elicit more layer 5 spiking. The dipole goes down, not up, in response to this input because most of the spiking in this case comes from the layer 5 basket cells, which hyperpolarize the somas of the layer 5 pyramidal cells and thus cause negative current.

On the other hand, the proximal 2 input induces a strong trough after the initial positive deflection. This trough is completely abolished when L-type calcium currents are blocked, and in fact its polarity is reversed (Figure 3.3B). The reason for this can be explained by examining some example voltage traces from each case (Figure 3.3C). Without calcium current, excitation simply enters in the basal dendrites and attenuates as it travels up the cell, from the soma to the apical dendrite, so the net current flow is upward. On the other hand, the inclusion of calcium currents which increase in maximum conductance toward the top of the cell causes a broad depolarization in the dendrite which then travels back down the cell and induces more spiking from the soma. This is a very illustrative example of how crucial accounting for calcium currents is to the model, particularly in simulations where the layer 5 pyramidal neurons are driven to spike. This was the case for proximal 1 as well, but because so few cells spiked at all this difference did not alter the dipole significantly.

One other notable feature of the proximal 2 input is that, with calcium currents included, the strength of this input mattered very little to the output waveform (and not at all for the qualitative behavior), at least within the 10%-200% range shown in Figure 3.3B, suggesting that the existence of a fairly synchronous calcium spike is sufficient to create a large stereotypical responses in the model dipole current. The input strength to the pyramidal cells is two orders of magnitude larger than that of proximal 1, so it is reasonable that even at 10% strength, the input is strong enough to induce an "all-or-nothing" response

of this form.

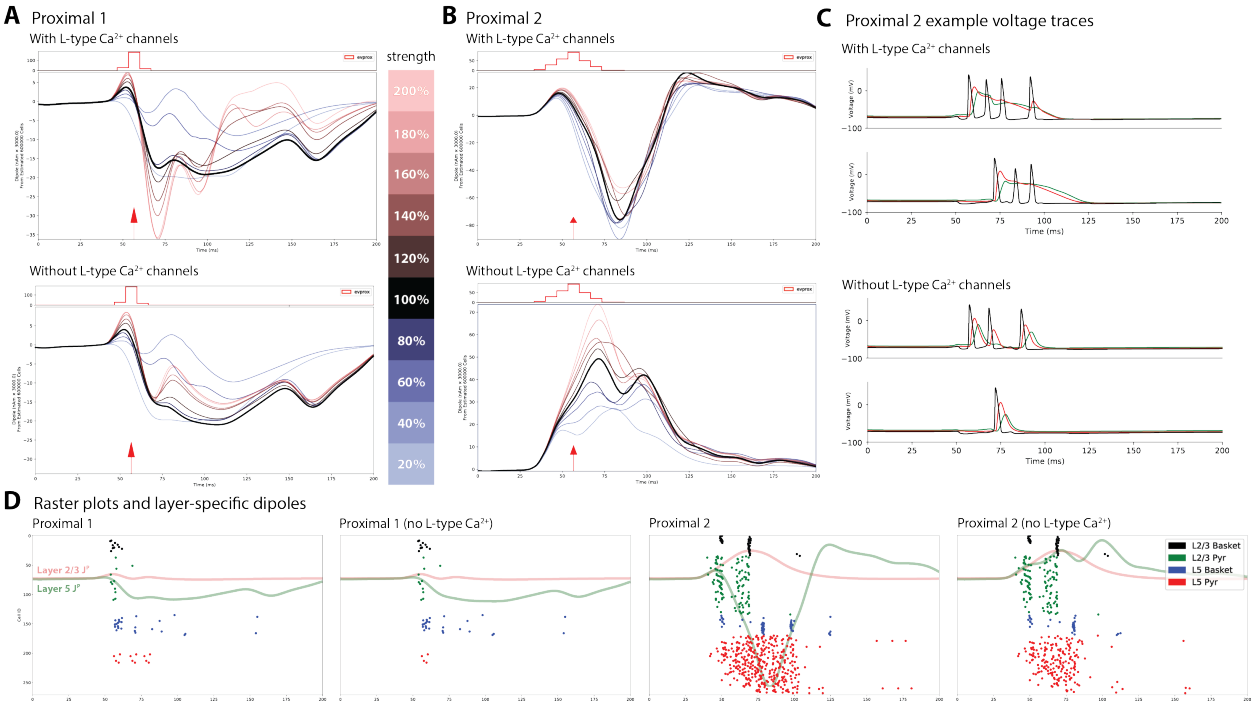

Figure 3.3: Response to feedforward excitation patterns. (**A**) Comparison of proximal 1 input with L-type calcium currents and without. The bolded black dipole signals are in response to the typical input. The thinner red and blue traces show the response when the input is scaled up or down in strength, according to the legend at right. (**B**) Comparison of proximal 2 input with L-type calcium currents and without, with the same color conventions as panel A. Notice the difference in y-axis scale between this panel and panel A. (**C**) Example voltage traces from layer 5 pyramidal neurons in response to proximal 2 are shown, with recordings from the soma (black), apical 2 (red), and apical tuft (green) from the same neuron overlaid. (**D**) Plots show spiking for each of the four cases at 100% strength, with the primary current dipole from layer 2/3 (pink) and layer 5 (green) overlaid. Black dots are L2/3 Basket spikes, green are L2/3 Pyr spikes, blue are L5 Basket spikes, and red are L5 Pyr spikes, consistent with the legend at right.

Though the Jones Lab typically focuses on the portion of an ERP shown in Figure 3.2 up to 170 ms, these results predicted that there should be a large dip immediately afterwards. However, when I reran the ERP simulations with the time window extended from 170 ms to 300 ms, I found that though there was a trough, it was nowhere near as negative as I expected it would be, and it was preceded by a significant positive shift (Figure 3.4A). Because dendritic calcium spikes have a long refractory period, the network which had already been driven to significant spiking activity was in a completely different dynamical state when the proximal 2 input arrived than the previously inactive network shown in Figure 3.3. The refractory period is the length of time after an event, such as a calcium or sodium spike, before another such event can be generated in the cell. Based on my simulations, for a proximal input, it takes about 125 ms after a prior calcium spike before any calcium is able to reenter the tuft, and about 160 ms before that amount is on a similar scale to the first calcium spike. In the example voltage traces (Figure 3.4A), I show one representative neuron

which does not fire a calcium spike in response to the distal input, so it does exhibit one in response to proximal 2, which would drive the dipole downward. Another representative neuron did produce a calcium spike in response to the distal input, and while it was able to produce a burst of back-propagating action potentials at the soma in response to proximal 2, it did not produce a dendritic calcium spike again. The contribution of these neurons to the dipole in response to proximal 2 was positive, as it was for the neurons in the no calcium current case of proximal 2 (Figure 3.3B and C). Of course, this was no longer very representative of a real ERP, as the time window was extended but no inputs from outside this modeled area were introduced during this added time. It is simply a good example of the effects of multiple successive excitatory inputs to the network.

To better understand these responses, I looked at the effects of a few different parameters in the calcium and no calcium conditions. The excitatory drive in proximal 2 takes place over a much more extended period of time than the proximal 1 input, so I was curious whether that had a large effect on the behavior. I switched the standard deviations of the two proximal inputs, both in the calcium and no calcium cases, and found that the standard deviation does not matter very much for the qualitative behavior in these cases. The main effect seems just to be a time shift. These results are shown in Figure 3.4B.

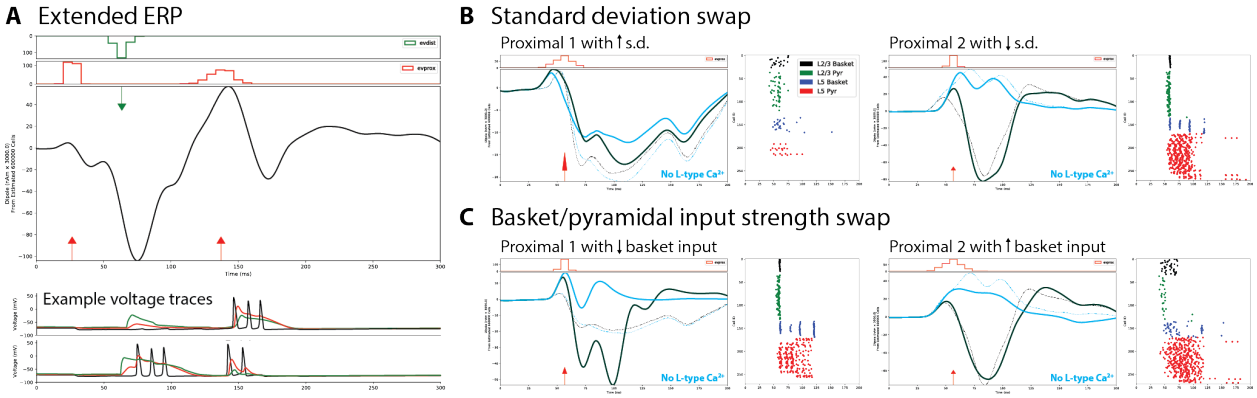

Figure 3.4: More investigations of feedforward inputs. (**A**) The same 3 ERP inputs as in Figure 3.2 but with the time window extended to 300 ms. As you can see, the response to proximal 2 does not look as it does in isolation (Figure 3.3B). In the example voltage traces below, black is from the soma, red is from apical 2, and green is from the apical tuft. (**B**) Dipoles from an input with proximal 1 strengths and proximal 2 standard deviation (left) and vice versa (right), cyan is without L-type calcium. (**C**) Dipole from an input with proximal 1 strengths to pyramidal cells and the basket cell strength scaled down to match the proximal 2 basket/pyramidal input strength ratio for each layer (left) and an input with proximal 2 strengths to pyramidal cells and the basket cell strength scaled up to match the proximal 1 basket/pyramidal input strength ratio for each layer (left). In both B and C, dotted traces are the original proximal 1 (left) and proximal 2 (right) responses, and light blue indicates the lack of L-type calcium currents. Rasters at right show spiking for the simulation represented by the solid black line in each condition.

Another variable is the relative input strength to the pyramidal cells versus the basket cells. Proximal 1 has a relatively stronger excitatory synaptic input to the basket cells than to the pyramidal cells, while proximal 2 has the reverse (this is true for both layers, see Table 3). In particular, the proximal input to layer 2/3 basket cells, which inhibit the somas

of layer 2/3 pyramidal cells and the distal dendrites of layer 5 pyramidal cells, is extremely weak compared to the other inputs in proximal 2. To investigate the importance of this difference, I switched the relative strengths of the excitation and inhibition by changing the level of excitatory synaptic drive from the proximal input to the basket cells. Consistent with my earlier results, I found that increasing the basket cell strength of the proximal 2 input was insufficient to stop the level of spiking seen in my previous simulations, so the dendritic calcium spikes occurred and the qualitative behavior was the same. On the other hand, decreasing the inhibition level in the proximal 1 input was enough to generate much more significant spiking in the layer 5 pyramidal, which caused the results from the calcium and no calcium case to more closely resemble the proximal 2 results (Figure 3.4C). The parameters used for these additional manipulations can be found in Table 4 at the end of the chapter.

3.3 Feedback excitation

The other input in the model ERP is a distal input. This is interpreted as a feedback input from a cortical region doing higher-level processing of the sensory stimulus that is then "fed back" to primary somatosensory cortex. This type of recurrent connection, by which downstream neurons modulate neurons receiving sensory signals, is extremely common in the brain.

The distal input in our ERP simulations produces a trough whose duration and amplitude are strongly modulated by the presence of L-type calcium currents (Figure 3.5). The strong input to the apical tufts of layer 5 pyramidal cells causes many of them to fire calcium spikes in the tuft, which drives current down and induces spiking in nearby neurons as well, so overall the current is very negative. In the case with no fast calcium current, there is an initial tuft-to-soma (downward) direction, but there are no calcium currents to sustain the depolarization and cause bursting. The cells spike once or twice, sending current back up the cell as the depolarization in the tuft decays, causing a quick recovery.

I also created an alternate distal input with different properties, so that I could do a similar analysis as I presented in the feedforward case, where I examined how different properties of the input determine the dipole's response and their dependencies on calcium. This input had the input strengths of proximal 1 but the longer standard deviation of proximal 2. The output is shown in Figure 3.5B. Interestingly, the result from this input matched much more closely to what we saw with the proximal 1 input. By looking at the voltage traces, I found that the reason for this is that the distal input to the layer 5 pyramidal cells was not strong enough to evoke significant electrical activity in the tuft that would cause a downward dipole. Instead, I could see that the spiking from these cells was evoked indirectly by excitation from the layer 2/3 pyramidal cells, which form synapses onto the basal and oblique dendrites of layer 5 pyramidal cells in addition to the distal dendrites. Because the layer 5 cells contribute more to the dipole than the layer 2 cells, the signal is dominated by the spiking that sends current up the dendrite, followed by the calcium activity in the tuft that sends it back down.

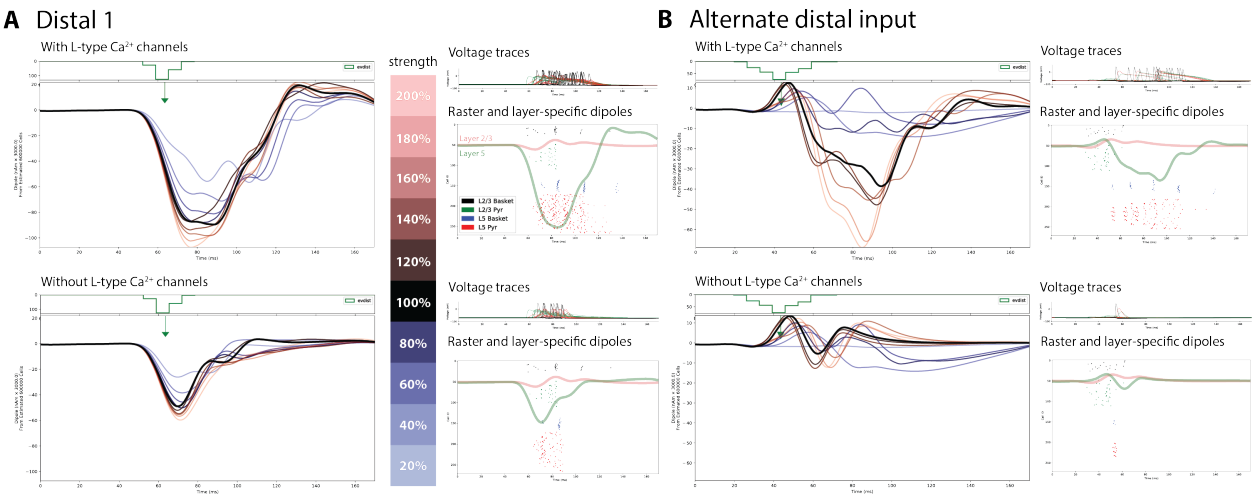

Figure 3.5: Response to feedback excitation patterns. (**A**) Comparison of distal 1 input with L-type calcium currents and without. The bolded black dipole signals are in response to the typical input. The thinner red and blue traces show the response when the input is scaled up or down in strength, according to the legend at right. The rasters at right show the spiking for the 100% strength input in each case, as well as the corresponding primary current dipoles from layer 2/3 (pink) and layer 5 (green). (**B**) Comparison of the alternate distal input with L-type calcium currents and without, with the same subplots and color conventions as panel A.

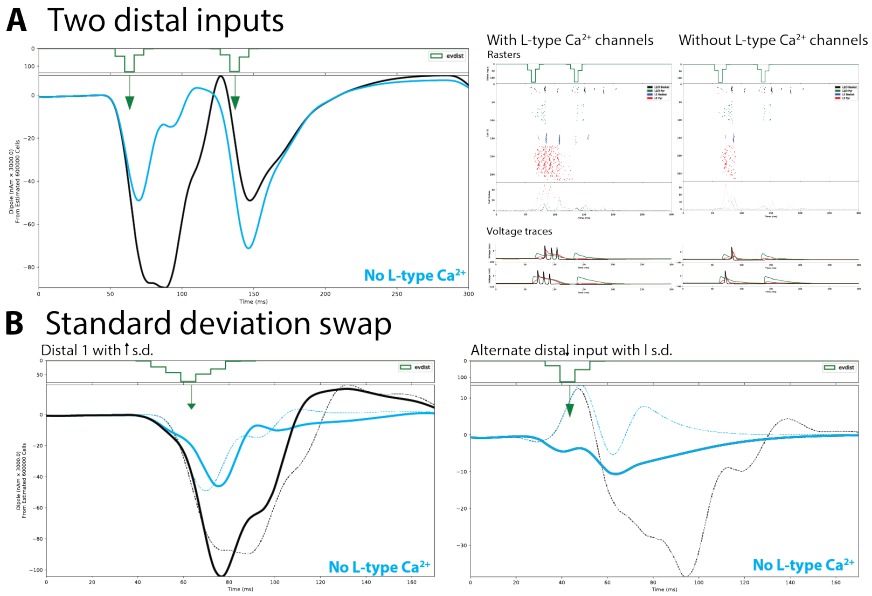

Figure 3.6: More investigations of feedback inputs. (**A**) Two distal inputs are presented in sequence (mean of 63.53 ms and 137.12 ms, respectively, to match distal 1 and proximal 2 in the full ERP simulations). From the plots you can see there was no spiking in response to the second input in either the calcium or no calcium case, but there is still a significant trough in the dipole. (**B**) Dipoles from an input with distal 1 strengths and alternate distal standard deviation (left) and vice versa (right).

Next, I ran simulations with two distal inputs in order to see the effect of a distal input after the network had already been activated, and once again how the refractory period

of calcium might play a role. For a distal input, the refractory period is somewhat longer than for a proximal input; it takes about 170 ms after a calcium spike for any distal input to generate, another, and for a threshold-level input to be able to evoke another spike, the latency is closer to 250 ms. As shown in Figure 3.6A, the layer 5 pyramidal cells were unable to spike again in response to the second input despite its being twice as strong as the first, but there was still a dip in response to this input due to the current being pushed down the tuft. The same phenomenon can be found in the case without calcium channels. In fact, this case has an even lower peak; however, after examination this appears to be only due to the fact that the dipole is less positive to begin with, combined with effects of the smoothing window.

Finally, I was again interested in how the standard deviation of the input affected dipole, as in the feedforward case. Broadening the standard deviation of the distal 1 input did not qualitatively change the results, but decreasing the standard deviation of the alternate distal input did end up changing the waveform drastically by stopping all spiking from the layer 5 pyramidal cells. The resulting waveform reflects a small amount of current traveling down the layer 5 dendrites, combined with a source from layer 2/3 pyramidal cells, which did produce spikes. The electrical activity was not strong enough to activate L-type calcium channels, so this waveform was the same in the case when these were present or absent.

3.4 Distal excitation with somatic inhibition

Lastly, I wanted to explore how the network responded when the distal excitatory inputs occurred at the same time as inhibitory inputs at the layer 5 pyramidal neuron somas, motivated by the idea that driving current down the cell and then stopping the spike in the soma could potentially create large electrical signatures without generating synaptic activity. This was a scenario that interested us because it was observed in the layer 2/3 pyramidal cells in Robert Law's study of how prestimulus beta events (a particular EEG waveform) affect ERPs [57]. When a beta event occurred within 100-400 ms before the tactile stimulus, the layer 2/3 cells responding to the tactile stimulus produced a spike in the dendrite, only to have it blocked at the soma due to inhibition evoked by the earlier beta event, causing a significant trough in the dipole without somatic spiking [57]. Since layer 5 pyramidal cells in the improved model produce calcium spikes, representing much broader electrical activity in the dendrites, we wanted to follow up by testing this input regime in this cell population.

To test this, I studied a more simplified layer 5 network response only, and created a simulation in which proximal and distal inputs only targeted layer 5 basket cells and layer 5 pyramidal cell apical tufts, respectively. First, I simulated a broad, strong drive to the basket cells to induce a great deal of spiking, which provides inhibitory synaptic inputs directly onto the somas of the layer 5 pyramidal cells (see Figure 3.7A top panel and blue spikes in the corresponding raster in figure 3.7B top panel). Subsequently, a distal input was delivered at 40% of the strength of the ERP distal input, but only to the layer 5 pyramidal cells. As you can see in Figure 3.7, this produces a trough in the dipole which is as deep as the trough created by the distal 1 input in the ERP, even though there is not any spiking from the layer 5 pyramidal cells at all.

The trough created by combining this distal input with inhibition is also slightly

deeper than the trough created by the distal input alone (without basket cell input), which produces widespread spiking in the layer 5 cells (Figure 3.7A, top panel). This is in some part because in the inhibited case, large currents are evoked in the dendrite, which travel down the cell and never trigger spikes. Spikes would backpropagate and send current back up the dendrite, as well as to the proximal dendrites of other layer 5 pyramidal cells through synapses. This creates upward current which would partially cancel out the downward flow. In other words, spiking sends current up and down many cells in the network over time, but distal excitation without spiking only sends the current down. By introducing inhibition, strong distal inputs that would have otherwise produced somatic spiking cannot, sending large amounts of current down the dendrites. Also, the inhibition at the soma causes it to hyperpolarize, which has a slight inhibitory effect on the dipole to begin with. As you can see from Figure 3.7, getting rid of calcium channels (with inhibition present) lessens this peak, because calcium currents increase the duration of the dendritic depolarizations and the resulting downward current deflection.

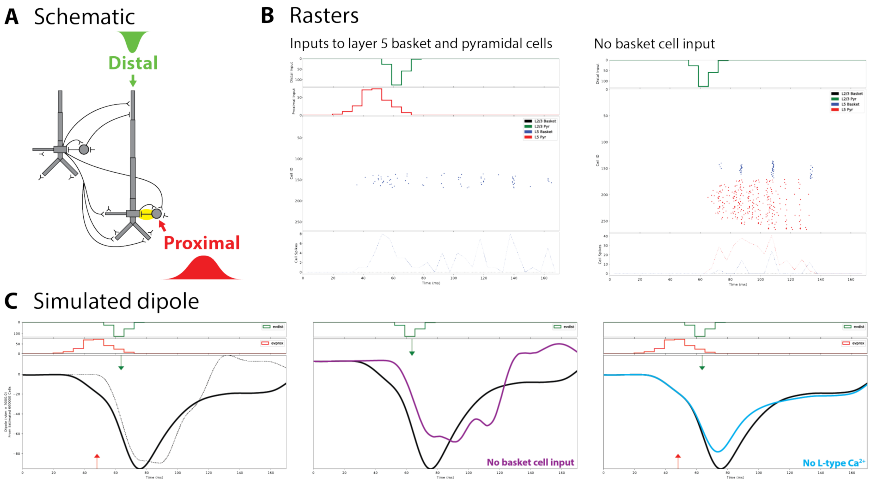

Figure 3.7: Distal excitation with somatic inhibition. (**A**) Schematic of the simulation experiment, showing the proximal input to L5 basket cells only and the distal input to L5 pyramidal cells only. The relevant inhibitory synapse is highlighted in yellow. (**B**) Raster plots corresponding to the simulations shown in panel C. The plot at left shows the spiking that corresponds to the solid black traces in panel C, and the plot at right corresponds to the no inhibition case represented in the second plot in panel A. (**C**) Simulations where layer 5 pyramidal cells received excitatory inputs to their apical tuft and inhibition to their somas via synaptic inputs from layer 5 basket cells. In all three plots, the solid black line is the control case. The dotted line in the first plot represents the distal 1 input discussed in the previous section. The purple and light blue lines in the next plots represent the simulation without basket cell input (somatic inhibition) and without L-type calcium currents, respectively.

The model of cortex is very complex and high-dimensional, but my study of the network's response to different types of inputs has shown a few guiding principles. The dipole signal is dominated by layer 5 pyramidal cells, and inducing calcium spikes in these cells creates long depolarizations in the apical tufts which send current down the dendrites and cause negative dipole signals. When there is strong inhibition at the soma, these currents will be strictly downward; otherwise, back-propagating action potentials will send current back up the cell, and other cells will also be excited synaptically. Repeated excitatory inputs

will not always be able to evoke another calcium spike in a cell which has already exhibited one recently, due to the refractory period of calcium, so in this case the dipole current will be more positive (in the case of a distal input it may make more sense to say less negative).

Other Inputs Used	↓ basket input prox 1	↑ basket input prox 2	Alternate distal	Second distal input	L5 Pyr somatic inhibition	L5 Pyr distal excitation
Start time standard deviation (ms)	2.47	8.33	8.33	3.85	8.5	3.85
Number of spikes per input	1	1	1	1	1	1
L2/3 Pyr AMPA weight (μS)	0.1525	1.44	0.01525	0.000014	0	0
L2/3 Pyr NMDA weight (μS)	0	0	0	0.0086	0	0
L2/3 Basket AMPA weight (μS)	0.00000003	8.34	0.08831	0.013	0	0
L2/3 Basket NMDA weight (μS)	0	0	0	0.04	0	0
L5 Pyr AMPA weight (μS)	0.00865	0.684	0.00865	0.285	0	0.057
L5 Pyr NMDA weight (μS)	0	0	0	0.16	0	0.032
L5 Basket AMPA weight (μS)	0.00011382	15.76			1	
L5 Basket NMDA weight (μS)	0	0			1	

Table 4: Evoked input parameters used in this chapter besides the three default ERP inputs. Mean start times varied between simulations, so they are not included. Inputs highlighted in red are proximal inputs, while inputs highlighted in green are distal inputs.

Chapter 4

Discussion

4.1 Summary

In this work, I adapted a model of cortical neurons to more accurately reproduce the dendritic calcium spiking in layer 5 pyramidal cells that has been observed in experimental recordings of these cells. The full model contains a scaleable network of compartmental model neurons whose electrical properties are governed by Hodgkin-Huxley-type differential equations, which describe the transmembrane ionic currents, and cable theory, which describes the propagation of currents within the cell (Chapter 1). By allowing the conductances of the ionic currents to vary continuously throughout the dendrites of these layer 5 cells, I was able to attain the broader, flatter dendritic spikes that have been reported in electrophysiological literature while still preserving the characteristic bursts of sodium-potassium action potentials in the soma (Section 2.2). After incorporating these adjusted neurons into the model network, I was able to qualitatively replicate the results of a 2017 paper which found that dendritic calcium spikes have a clear signature in surface electrode recordings from rats [30] (Section 2.3). I then subjected this model to a more general exploration to investigate how calcium spiking in these dendrites affects the simulated source-localized EEG signal in response to realistic input paradigms that have been used to reproduce ERP data (Chapter 3). I found that the long-lasting dendritic depolarization characteristic of a calcium spike drives current down the apical dendrite, causing overall more negative deflections in the dipole than the corresponding simulations without these L-type calcium currents. Because calcium spikes that accompany somatic bursts are "all-or-nothing" events in the model with a fairly consistent length, an input which is able to drive many simultaneous calcium spikes creates a dipole output that is similarly invariant to the strength of the input so long as it is above that threshold. However, because of the relatively long refractory period of calcium spiking in the distal dendrite (on the order of 150-250 ms), a strong input does not guarantee simultaneous calcium spiking if the network is already in an excited state.

4.2 Significance

First, this work is important to our lab's efforts because it improves the fit of the model cortex to experimental findings. This change did not require the introduction of any new mecha-

nisms or added complexity, only changing the conductance values of several ionic currents. Thus, there is no significant downside to adopting this model, and it will be adapted into the Human Neocortical Neurosolver software that the lab distributes (https://hnn.brown.edu). I have also corroborated work that has found that dendritic calcium spikes are visible in surface electrode recordings, as well as using the model's ability to record spiking behavior, voltage traces, and calcium dynamics from each of the cells to demonstrate why these surface recordings of calcium spikes look the way they do and why they are abolished by the $GABA_B$ agonist baclofen in layers 2 and 3.

Moreover, my work has potentially significant implications for how we understand the effect of dendritic electrical properties on EEG and MEG signals. Because it is infeasible to record the underlying activity of human neurons while conducting EEG, the use of a model provides an important way to gain an understanding of how cellular dynamics affect macroscale signals from these noninvasive methods. My results indicate that the presence or absence of coordinated dendritic calcium spiking may affect the dipole signal more than we had previously known or expected. The presence of this coordinated spiking should result in a large, stereotyped waveform reflective of current which originates in the distal dendrites and propagates downward to the soma. I believe that understanding this phenomenon will aid future insights into the connection between network activity and EEG markers of different healthy and pathological states.

4.3 Limitations

4.3.1 Differences between rodent and human neocortex

One issue with this work, particularly the redistribution of ion channels detailed in Chapter 2, is I was fitting the data mostly to data from mouse and rat pyramidal neurons. For obvious reasons, there are very, very few electrophysiology experiments performed with human neurons, especially *in vivo*. In many respects, mice and rats are good model systems for studying human neocortex since they have the same six-layer structure. However, their brains are smooth, not folded, and their pyramidal neurons are much smaller in these animals and may differ from ours in important ways. Recent work suggests that humans' layer 2/3 pyramidal neurons may have more excitable dendrites than rodents', and our layer 5 pyramidal neurons may be more electrically compartmentalized with less active conductances [28, 1]. Active dendritic conductances are just beginning to be studied in humans, so there is not enough data yet to reliably fit our model to the human brain. Until there is more experimental work done, it will not be possible to ensure that we are not missing some critical variable. Nonetheless, based on this early work, I expect that the improved model I have created is closer to real human dendritic activity than the original model, and is therefore a step in the right direction.

4.3.2 Potential importance of other cell types

EEG currents are dominated by the electrical activity in the two classes of pyramidal cells, but the activity of other cell types, especially inhibitory interneurons, has a huge impact on

the state of the network as a whole and the signals that emerge from the pyramidal cells. The Jones Lab model includes two inhibitory cell populations, both of which are basket cells, which are fast-spiking and provide strong inhibition at pyramidal cell somas. Basket cells make up about half of all inhibitory interneurons [58], but other types of interneurons, including Martinotti cells and neurogliaform cells, may be important for our understanding of EEG networks. These subtypes have distinct properties: for example, Martinotti cells have long axons that can inhibit the distal dendrites of neurons millimeters away [58]. In Law's study of beta events, he added extra "Martinotti-like" connections from the layer 5 basket cells to the apical tufts of the layer 5 pyramidal neurons in order to simulate this source of inhibition, but no new inhibitory populations have been added to the model outright [57]. With my focus on the electrical activity in the dendrites, it is possible that adding a new inhibitory cell type targeting these dendrites would better model the real brain and change the response of the network to the evoked inputs explored in Chapter 3.

4.3.3 High dimensionality and large parameter space

The lack of certain inhibitory cell populations is just one of the many ways in which this model is simplifying some aspect of the real brain. I could spend pages and pages of this section talking about ways that we could add to this model. In truth though, this model is already extremely complex. In fact, in a simulation with three evoked inputs as in the ERP dipoles, there are over 250 parameters that can be simply changed by the user by changing their value in the input file. These parameters characterize cell size, cell biophysics, synaptic strengths, network dimensions, and input characteristics. And these do not even include a number of parameters which are inherent in the model, such as the many parameters in the differential equations that describe the kinetics of ion channels.

In addition, there is a huge number of complex and interdependent differential equations that describe the system. Even a classical Hodgkin-Huxley point neuron is described by a system of four equations. The default Jones Lab model, representing a cortical column consisting of 200 pyramidal cells which each have many types of ion channels and cable equations that must be solved along the length of the compartments, is an extremely high-dimensional system.

This complexity of this system is great for approximating the real brain and trying to fit directly to EEG data. The cost is that it makes the system very hard to analyze and understand. First of all, the high dimensionality of the system of differential equations make it very difficult to generate any mathematical insights about the behavior of the system without simply running the simulations and studying what happens. This has rendered me unable to make any mathematical or theoretical claims about the impact of calcium currents in my new version of the model beyond what can be understood from looking at the simulation data. Even if you are not trying to understand the model from a theoretical point of view, and are just trying to use the model to understand something about your data, for example why children's auditory ERPs look different than adults' [59], the huge parameter space to contend with makes it difficult to tune the model and ensure your tuning makes sense unless you have a strong understanding ahead of time about what cellular and network mechanisms might be involved. Other lab members are currently trying to better characterize these parameters' effects and interdependencies through sensitivity analysis, and

to use that knowledge to find more efficient ways to optimize parameter values while ensuring biological accuracy. Ultimately, though, this model is inherently very large and complex, and to some extent it will always be a feature of this model that biophysical accuracy is traded for intuition about system behavior and parameter effects.

4.4 Future directions

4.4.1 Similar improvements to layer 2/3 pyramidal cells

I have been focusing my efforts on layer 5 pyramidal cells because they contribute significantly more to the dipole and because there has been much more experimental research into calcium spiking and other active dendritic properties in this cell type than in the layer 2/3 pyramidal cells. This second point is mostly due to the fact that layer 5 pyramidal dendrites are easier to record from, since they are thicker [60]. In a 2007 paper, Larkum et al. found that layer 2/3 pyramidal cells in rats also exhibit dendritic spikes associated with calcium, although they reported that these cells do not exhibit the long "plateau potentials" exhibited in layer 5 cells [60]. Earlier this year, a paper came out that actually looked at dendritic action potentials in human layer 2/3 pyramidal neurons [28]. Not only do these neurons exhibit dendritic calcium spikes, but it appears they have graded properties that have not been reported previously reported in the rodent literature, i.e. that rather than being an all-or-none response, these currents respond maximally to threshold-level inputs and dampen for stronger stimuli [28]. These results are very preliminary, but it is clear that there is at least some calcium activity in human layer 2/3 pyramidal cells. The Jones Lab model currently does not include any calcium currents in this cell type. A good next step would be to add these currents in and use the insights from this work to tune the dendritic conductances to the available data from rodents and humans.

4.4.2 More detailed model of calcium dynamics

Hot zones

In the model I have implemented, calcium channels increase linearly along the dendrite before plateauing in the tuft. This monotonic change was based on the modeling work of Almog and Korngreen [42], and it was chosen because it produced behavior that fit well to the data. However, other modeling work has incorporated a so-called calcium hot zones, areas of high calcium channel density on the distal apical dendrite just before it branches significantly to form the tuft in layer 1 where dendritic calcium [61, 41, 62]. Though in our model it has been simplified to one compartment, the apical tuft of a dendrite actually splits into many branches which can receive many inputs. The idea is that when these branches come together in the calcium hot zone, these inputs sum, and if the total input is sufficiently excitatory to engage these high voltage activated channels, a dendritic calcium spike is evoked. The experimental evidence for this is somewhat unclear to me; it has been claimed that there is an initiation zone in this area, but these studies do not actually record from the branches of the tuft, presumably because they are much thinner and thus more difficult to insert an electrode into [45, 26]. Early on in my quest to find a good distribution of ion channels, I

experimented with including a hot zone, without any promising results. However, now that I have found a good baseline model, it may be worth another attempt. This would be done by introducing a region of high calcium conductance toward the top of apical 2, then having the calcium conductance decrease again into the tuft.

Buffering and other calcium interactions

After finding that calcium diffusion alone was not enough to account for the differences between our model and the experimental data, I moved away from thinking about the role of calcium ions within the cell and turned my attention to transmembrane currents and conductances. I now believe that understanding and modeling these currents is the key to finding a realistic neuronal model in this context, and that achieving biological accuracy in this respect is probably as detailed as we need to be our purposes, since often it is broad trends like directionality of current and amount of spiking in a given cell population that matter for our applications. The Jones Lab model (both my updated version and the original model) includes two types of calcium currents, L-type and T-type, as well as a simple calcium pump which causes intracellular calcium concentration to decay over time at a rate specified by the user [6]. However, as I addressed in Section 2.2.3, calcium ions play a very unique role in the cell. These ions undergo buffering reactions, can be stored and released by the endoplasmic reticulum, and are involved in molecular cascades. It is possible that buffering and calcium storage could affect the results by changing the intracellular calcium concentration. This could be investigated using the reaction-diffusion model that I worked with in an earlier stage of this project [37].

4.4.3 Direct comparison to experimental EEG data

In this work, I have examined experimental electrophysiology data in order to tune the calcium dynamics and electrical activity in the layer 5 pyramidal cells. After I settled on a model that I felt did a good job of capturing these experimental phenomena, my work has been purely in creating simulations and interpreting model results in terms of model construction and parameters. The actual intent, however, of the Jones Lab model is to compare model output (current dipole) to source-localized EEG or MEG data from experimental or clinical settings.

Perception and attention tasks

The experiments done in our lab deal with tactile perception and attention. We already have datasets from studies looking at somatosensory ERPs for hit and miss trials in tasks that asked subjects to report when they felt a threshold-level tap to the finger, as well as tasks in which subjects were asked to pay attention to either their hand or their foot (giving "attend-in" and "attend-out" conditions in the hand area of primary somatosensory cortex).

The ERP inputs discussed in Chapter 3 were useful for determining general principles for the network responded to inputs of different strengths and properties, as applied to my new model they give an ERP which has a qualitatively correct profile but which differs from

the lab's default model in a few important ways, most notably exhibiting a lower trough in response to the distal input.

Going forward, we hope to incorporate the improvements I have made into the general Jones Lab model and distribute it with the HNN software. This will require tuning a sequence of inputs that more closely matches our data from perception and attention models. I expect that the general sequence of inputs (proximal 1, distal, proximal 2) will be preserved, as well as the biological interpretation that these inputs represent an incoming signal, a feedback response, and then by general somatosensory excitation caused by a thalamaocortical loop. However, the input strengths and the timings will most likely need to be tuned.

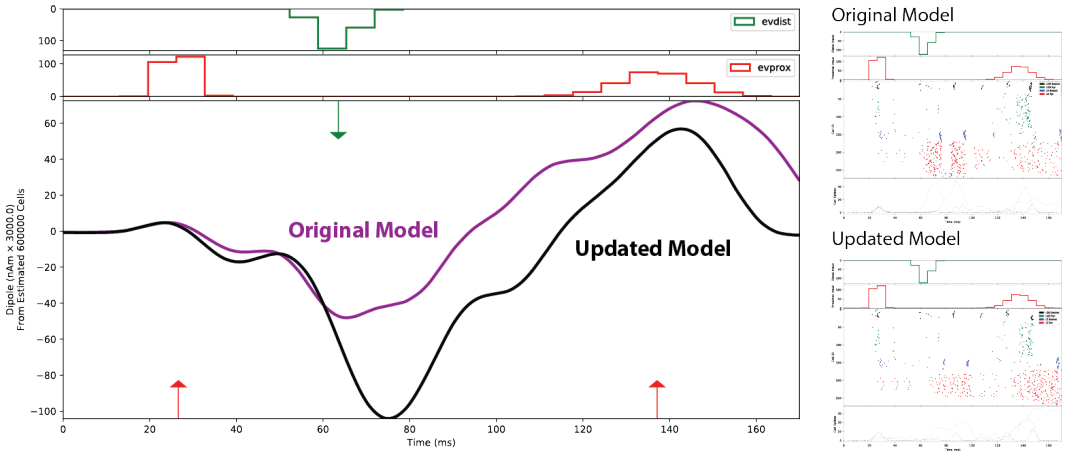

Comparison of response to ERP inputs in the original model versus my updated model. At left, the two dipoles are overlaid, with the output of the original model in purple. The most notable difference with my new model is the much larger trough in response to the distal input. At right, the raster plots corresponding to each input are shown. My updated model produces less spiking in response to the distal input, and more in response to the second proximal input.

Transcranial magnetic stimulation

Transcranial magnetic stimulation (TMS) is a noninvasive method of stimulating the brain from outside the head, using a magnetic coil to apply brief but strong magnetic pulses to the brain [63]. These pulses evoke electrical activity in the underlying tissue. TMS is an FDA-approved intervention for treatment-resistant depression and obsessive-compulsive disorder and certain types of migraines [64], and is being actively researched in other clinical applications including treatment of schizophrenia, stroke, and Alzheimer's disease [65, 66, 67]. However, its neural effects at the cellular and circuit level are not well understood [63].

Our lab has taken a recent interest in TMS used in combination with EEG. One ongoing project is to run a simple tactile detection task used in prior studies, where people are asked to report whether or not they can feel a very light tap to their fingers, concurrent with either sham or actual TMS, to examine the effects of TMS stimulation on detection and on the ERP waveforms. Given our modeling work, this can help to understand what TMS is actually doing at the circuit level if we can make parameter changes from the control condition that account for the TMS results.

Dendritic calcium dynamics in layer 5 pyramidal cells are potentially very important to the effects of TMS. Murphy et al. performed TMS with simultaneous calcium imaging in rats who were presented with tactile stimuli to their hindpaws *in vivo* [68]. They found that TMS abolished the dendritic calcium spike that was normally observed in response to the hindpaw stimulation, an effect most likely mediated by recruitment of strong inhibition [68]. Di Lazzaro, Rothwell, and Capogna have speculated that TMS recruits neurogliaform cells, which is in line with this work because these cells provide inhibition primarily to the apical tufts and distal tufts of laery 5 pyramidal neurons [63]. Especially since their use of hindpaw stimuli is fairly analogous to our use of finger taps, we may find similar results in modeling the TMS ERP data. I believe that my work on improving the model of dendritic electrical activity has lain the groundwork for further study of this relationship using our model and the data from TMS-EEG experiments.

4.5 Conclusion

This research has linked many scales of modeling and analysis, from models of individual ion channels, to simulated and recorded voltage traces in pyramidal cells, to network spiking activity and dynamics, and finally to a dipole signal which reflects the activity of tens of thousands of cells. The next step is to apply this work to fit real EEG data, to connect this large scale signal to experimental evidence. Given the importance of dendritic calcium spiking for the dipole signal in my simulations, I believe this last step in the process will generate new explanations and hypotheses about how EEG signals are reflective of cellular activity.

4.6 Acknowledgements

I would like to thank Dr. Stephanie Jones from the bottom of my heart for welcoming me into the lab and being so incredibly supportive of my research over the years, even as I have often doubted that I was doing anything useful. She is a wonderful person as well as an amazing scientist. I would like to thank Dr. Robert Law for all of the time he took introducing me to the model and getting me started on the work that ultimately became this research project, and Dr. Samuel Neymotin for his patient help with my many technical difficulties. I am truly thankful for the entire Jones Lab; I could not have asked for a better undergraduate research experience. In addition, I would like to thank Dr. Matthew Harrison for taking me on as an advisee and being so encouraging of my mathematical endeavors, Dr. Monica Linden for convincing me that I am a math student at heart, and Dr. Christopher Moore for his wisdom and infectious enthusiasm for science. Lastly, I owe so many thanks to my parents for their endless love and support.

Bibliography

[1] Lou Beaulieu-Laroche, Enrique H.S. Toloza, Marie Sophie van der Goes, Mathieu Lafourcade, Derrick Barnagian, Ziv M. Williams, Emad N. Eskandar, Matthew P. Frosch, Sydney S. Cash, and Mark T. Harnett. Enhanced Dendritic Compartmentalization in Human Cortical Neurons. *Cell*, 175(3):643–651, 10 2018.

[2] Electrocorticography (ECoG).

[3] Abraham Kuruvilla and Roland Link. Intraoperative electrocorticography in epilepsy surgery: useful or not? *Seizure - European Journal of Epilepsy*, 12(8):577–584, 12 2003.

[4] P Shenoy, K J Miller, J G Ojemann, and R P N Rao. Generalized Features for Electrocorticographic BCIs. *IEEE Transactions on Biomedical Engineering*, 55(1):273–280, 2008.

[5] Fritjof Helmchen, Karel Svoboda, Winfried Denk, and David W Tank. In vivo dendritic calcium dynamics in deep-layer cortical pyramidal neurons. *Nature Neuroscience*, 2(11):989–996, 11 1999.

[6] Samuel A Neymotin, Dylan S Daniels, Blake Caldwell, Robert A McDougal, Nicholas T Carnevale, Mainak Jas, Christopher I Moore, Michael L Hines, Matti Hämäläinen, and Stephanie R Jones. Human Neocortical Neurosolver (HNN), a new software tool for interpreting the cellular and network origin of human MEG/EEG data. *eLife*, 9, 1 2020.

[7] David Cohen and B.Neil Cuffin. Demonstration of useful differences between magnetoencephalogram and electroencephalogram. *Electroencephalography and Clinical Neurophysiology*, 56(1):38–51, 1983.

[8] Winston Chiong, Matthew K Leonard, and Edward F Chang. Neurosurgical Patients as Human Research Subjects: Ethical Considerations in Intracranial Electrophysiology Research. *Neurosurgery*, 83(1):29–37, 7 2017.

[9] Alan L Hodgkin, Andrew F Huxley, and Bernard Katz. Measurement of current-voltage relations in the membrane of the giant axon of Loligo. *The Journal of physiology*, 116(4):424–448, 1952.

[10] The Nobel Prize in Physiology or Medicine 1963, 2020.

[11] Peter Dayan and Laurence F Abbott. *Theoretical neuroscience: computational and mathematical modeling of neural systems*. MIT Press, Cambridge, MA, 2001.

[12] L F Abbott and Thomas B Kepler. Model neurons: from Hodgkin-Huxley to Hopfield. In *Statistical Mechanics of Neural Networks*, pages 5–18. Springer, 1990.

[13] Wilfrid Rall. Branching dendritic trees and motoneuron membrane resistivity. *Experimental neurology*, 1(5):491–527, 1959.

[14] Wilfrid Rall. Theory of physiological properties of dendrites. *Annals of the New York Academy of Sciences*, 96(4):1071–1092, 1962.

[15] Wilfrid Rall. Core conductor theory and cable properties of neurons. *Comprehensive physiology*, pages 39–97, 2011.

[16] Wilfrid Rall. Theoretical Significance of Dendritic Trees for Neuronal Input-Output Relations (1964). In R.F. Reiss, editor, *Neural Theory and Modeling*, chapter 4.2, pages 122–146. Stanford University Press, Stanford, CA, 1964.

[17] M L Hines and N T Carnevale. The NEURON Simulation Environment. *Neural Computation*, 9(6):1179–1209, 8 1997.

[18] C Koch, R Douglas, and U Wehmeier. Visibility of synaptically induced conductance changes: theory and simulations of anatomically characterized cortical pyramidal cells. *The Journal of Neuroscience*, 10(6):1728, 6 1990.

[19] Michael L Hines, Andrew P Davison, and Eilif Muller. NEURON and Python. *Frontiers in Neuroinformatics*, 3:1–12, 1 2009.

[20] Stephanie R. Jones, Dominique L. Pritchett, Steven M. Stufflebeam, Matti Hämäläinen, and Christopher I. Moore. Neural correlates of tactile detection: A combined magnetoencephalography and biophysically based computational modeling study. *Journal of Neuroscience*, 27(40):10751–10764, 10 2007.

[21] Paul C. Bush and Terrence J. Sejnowski. Reduced compartmental models of neocortical pyramidal cells. *Journal of Neuroscience Methods*, 46(2):159–166, 1993.

[22] Stephanie R. Jones, Dominique L. Pritchett, Michael A. Sikora, Steven M. Stufflebeam, Matti Hämäläinen, and Christopher I. Moore. Quantitative analysis and biophysically realistic neural modeling of the MEG mu rhythm: Rhythmogenesis and modulation of sensory-evoked responses. *Journal of Neurophysiology*, 102(6):3554–3572, 12 2009.

[23] Shane Lee and Stephanie R. Jones. Distinguishing mechanisms of gamma frequency oscillations in human current source signals using a computational model of a laminar neocortical network. *Frontiers in Human Neuroscience*, 7, 12 2013.

[24] Maxwell A. Sherman, Shane Lee, Robert Law, Saskia Haegens, Catherine A. Thorn, Matti S. Hämäläinen, Christopher I. Moore, and Stephanie R. Jones. Neural mechanisms of transient neocortical beta rhythms: Converging evidence from humans, computational modeling, monkeys, and mice. *Proceedings of the National Academy of Sciences*, 113(33):E4885–E4894, 8 2016.

[25] Jackie Schiller, Yitzhak Schiller, Greg Stuart, and Bert Sakmann. Calcium action potentials restricted to distal apical dendrites of rat neocortical pyramidal neurons. *Journal of Physiology*, 505(3):605–616, 12 1997.

[26] Matthew E Larkum and J Julius Zhu. Signaling of layer 1 and whisker-evoked Ca2+ and Na+ action potentials in distal and terminal dendrites of rat neocortical pyramidal neurons in vitro and in vivo. *The Journal of neuroscience : the official journal of the Society for Neuroscience*, 22(16):6991–7005, 8 2002.

[27] Enrique Pérez-Garci, Martin Gassmann, Bernhard Bettler, and Matthew E. Larkum. The GABAB1b Isoform Mediates Long-Lasting Inhibition of Dendritic Ca2+ Spikes in Layer 5 Somatosensory Pyramidal Neurons. *Neuron*, 50(4):603–616, 5 2006.

[28] Albert Gidon, Timothy Adam Zolnik, Pawel Fidzinski, Felix Bolduan, Athanasia Papoutsi, Panayiota Poirazi, Martin Holtkamp, Imre Vida, and Matthew Evan Larkum. Dendritic action potentials and computation in human layer 2/3 cortical neurons. Technical report.

[29] Diane Lipscombe, Thomas D Helton, and Weifeng Xu. L-Type Calcium Channels: The Low Down. *Journal of Neurophysiology*, 92(5):2633–2641, 11 2004.

[30] Mototaka Suzuki and Matthew E. Larkum. Dendritic calcium spikes are clearly detectable at the cortical surface. *Nature Communications*, 8(1), 12 2017.

[31] L R Silva, M J Gutnick, and B W Connors. Laminar distribution of neuronal membrane properties in neocortex of normal and reeler mouse. *Journal of Neurophysiology*, 66(6):2034–2040, 12 1991.

[32] J Julius Zhu and Barry W Connors. Intrinsic Firing Patterns and Whisker-Evoked Synaptic Responses of Neurons in the Rat Barrel Cortex. *Journal of Neurophysiology*, 81(3):1171–1183, 3 1999.

[33] Elizabeth A Matthews and Dirk Dietrich. Buffer mobility and the regulation of neuronal calcium domains. *Frontiers in cellular neuroscience*, 9:48, 2 2015.

[34] Aaron L Fogelson and Robert S Zucker. Presynaptic calcium diffusion from various arrays of single channels. Implications for transmitter release and synaptic facilitation. *Biophysical journal*, 48(6):1003, 1985.

[35] Robert S Zucker and Norman Stockbridge+. Presynaptic calcium diffusion and the time courses of transmitter release and synaptic facilitation at the squid giant synapse. Technical Report 6, 1983.

[36] M. C. Nowycky and M. J. Pinter. Time courses of calcium and calcium-bound buffers following calcium influx in a model cell. *Biophysical Journal*, 64(1):77–91, 1993.

[37] Robert A. McDougal, Michael L. Hines, and William W. Lytton. Reaction-diffusion in the NEURON simulator. *Frontiers in Neuroinformatics*, 7, 2013.

[38] Amrita Tripathi and Neeru Adlakha. Finite Volume Model to Study Calcium Diffusion in Neuron Involving J RYR , J SERCA and J LEAK. Technical report, 2011.

[39] Armin Biess, Eduard Korkotian, and David Holcman. Barriers to diffusion in dendrites and estimation of calcium spread following synaptic inputs. *PLoS Computational Biology*, 7(10), 10 2011.

[40] F. Sala and A. Hernández-Cruz. Calcium diffusion modeling in a spherical neuron. Relevance of buffering properties. *Biophysical Journal*, 57(2):313–324, 1990.

[41] Adam S. Shai, Costas A. Anastassiou, Matthew E. Larkum, and Christof Koch. Physiology of Layer 5 Pyramidal Neurons in Mouse Primary Visual Cortex: Coincidence Detection through Bursting. *PLoS Computational Biology*, 11(3), 3 2015.

[42] M. Almog and A. Korngreen. A Quantitative Description of Dendritic Conductances and Its Application to Dendritic Excitation in Layer 5 Pyramidal Neurons. *Journal of Neuroscience*, 34(1):182–196, 1 2014.

[43] Rafael Yuste, Michael J Gutnick, Drorit Saar, Kerry R Delaney, and David W Tank. Ca2+ accumulations in dendrites of neocortical pyramidal neurons: An apical band and evidence for two functional compartments. *Neuron*, 13(1):23–43, 1994.

[44] Alon Korngreen and Bert Sakmann. Voltage-gated K+ channels in layer 5 neocortical pyramidal neurones from young rats: subtypes and gradients. *The Journal of Physiology*, 525(3):621–639, 6 2000.

[45] M E Larkum, J J Zhu, and B Sakmann. Dendritic mechanisms underlying the coupling of the dendritic with the axonal action potential initiation zone of adult rat layer 5 pyramidal neurons. *The Journal of Physiology*, 533(2):447–466, 6 2001.

[46] M E Larkum, K M Kaiser, and B Sakmann. Calcium electrogenesis in distal apical dendrites of layer 5 pyramidal cells at a critical frequency of back-propagating action potentials. *Proceedings of the National Academy of Sciences of the United States of America*, 96(25):14600–14604, 12 1999.

[47] Stephen R Williams and Greg J Stuart. Backpropagation of physiological spike trains in neocortical pyramidal neurons: implications for temporal coding in dendrites. *Journal of Neuroscience*, 20(22):8238–8246, 2000.

[48] Yael Chagnac-Amitai, Heiko J Luhmann, and David A Prince. Burst generating and regular spiking layer 5 pyramidal neurons of rat neocortex have different morphological features. *Journal of Comparative Neurology*, 296(4):598–613, 1990.

[49] Peter Schwindt and Wayne Crill. Mechanisms underlying burst and regular spiking evoked by dendritic depolarization in layer 5 cortical pyramidal neurons. *Journal of Neurophysiology*, 81(3):1341–1354, 1999.

[50] Steven J Luck, Geoffrey F Woodman, and Edward K Vogel. Event-related potential studies of attention. *Trends in cognitive sciences*, 4(11):432–440, 2000.

[51] Michelle De Haan, Mark H Johnson, and Hanife Halit. Development of face-sensitive event-related potentials during infancy: a review. *International Journal of Psychophysiology*, 51(1):45–58, 2003.

[52] David Friedman and Ray Johnson Jr. Event-related potential (ERP) studies of memory encoding and retrieval: A selective review. *Microscopy research and technique*, 51(1):6–28, 2000.

[53] Anke Karl, Loretta S Malta, and Andreas Maercker. Meta-analytic review of event-related potential studies in post-traumatic stress disorder. *Biological psychology*, 71(2):123–147, 2006.

[54] Jarmo A Hämäläinen, Hanne K Salminen, and Paavo H T Leppänen. Basic auditory processing deficits in dyslexia: systematic review of the behavioral and event-related potential/field evidence. *Journal of learning disabilities*, 46(5):413–427, 2013.

[55] Walter S Pritchard. Cognitive event-related potential correlates of schizophrenia. *Psychological bulletin*, 100(1):43, 1986.

[56] Danielle D. Sliva, Christopher J. Black, Paul Bowary, Uday Agrawal, Juan F. Santoyo, Noah S. Philip, Benjamin D. Greenberg, Christopher I. Moore, and Stephanie R. Jones. A prospective study of the impact of transcranial alternating current stimulation on EEG correlates of somatosensory perception. *Frontiers in Psychology*, 9(NOV), 11 2018.

[57] Robert G Law, Sarah Pugliese, Hyeyoung Shin, Danielle Sliva, Shane Lee, Samuel Neymotin, Christopher Moore, and Stephanie R Jones. A supragranular nexus for the effects of neocortical beta events on human tactile perception. *bioRxiv*, page 750992, 2019.

[58] Henry Markram, Maria Toledo-Rodriguez, Yun Wang, Anirudh Gupta, Gilad Silberberg, and Caizhi Wu. Interneurons of the neocortical inhibitory system. *Nature Reviews Neuroscience*, 5(10):793–807, 2004.

[59] Donna Coch, Wendy Skendzel, and Helen J. Neville. Auditory and visual refractory period effects in children and adults: An ERP study. *Clinical Neurophysiology*, 116(9):2184–2203, 9 2005.

[60] Matthew Evan Larkum, Jack Waters, Bert Sakmann, and Fritjof Helmchen. Dendritic spikes in apical dendrites of neocortical layer 2/3 pyramidal neurons. *Journal of Neuroscience*, 27(34):8999–9008, 8 2007.

[61] Etay Hay, Sean Hill, Felix Schürmann, Henry Markram, and Idan Segev. Models of Neocortical Layer 5b Pyramidal Cells Capturing a Wide Range of Dendritic and Perisomatic Active Properties. *PLoS Computational Biology*, 7(7):e1002107, 7 2011.

[62] Matthew E Larkum, Thomas Nevian, Maya Sandler, Alon Polsky, and Jackie Schiller. Synaptic Integration in Tuft Dendrites of Layer 5 Pyramidal Neurons: A New Unifying Principle. *Science*, 325(5941):756, 8 2009.

[63] Vincenzo Di Lazzaro, John Rothwell, and Marco Capogna. Noninvasive Stimulation of the Human Brain: Activation of Multiple Cortical Circuits, 6 2018.

[64] FDA permits marketing of transcranial magnetic stimulation for treatment of obsessive compulsive disorder — FDA.

[65] Bianca Graziano, Rachel E. Kaskie, and Fabio Ferrarelli. Transcranial Magnetic Stimulation (TMS) as a treatment tool in schizophrenia: A review., 2017.

[66] Marie Claire Smith and Cathy M. Stinear. Transcranial magnetic stimulation (TMS) in stroke: Ready for clinical practice?, 9 2016.

[67] Stephanie S. Buss, Peter J. Fried, and Alvaro Pascual-Leone. Therapeutic noninvasive brain stimulation in Alzheimers disease and related dementias. *Current Opinion in Neurology*, 32(2):292–304, 4 2019.

[68] Sean C. Murphy, Lucy M. Palmer, Thomas Nyffeler, René M. Müri, and Matthew E. Larkum. Transcranial magnetic stimulation (TMS) inhibits cortical dendrites. *eLife*, 5(MARCH2016), 3 2016.